

國立臺灣大學理學院化學所

碩士論文

Graduate Institute of Chemistry

College of Science

National Taiwan University

Master Thesis



7-Azaindole 及相似物之水催化激發態質子轉移反應
Water-Catalyzed Excited-State Proton Transfer Reactions
in 7-Azaindole and Its Analogues

吳毓心

Yu-Sin Wu

指導教授：周必泰 博士

Advisor: Pi-Tai Chou, Ph.D.

中華民國 103 年 7 月

July 2014



謝辭

兩年的碩班真的學到很多，與大學同樣都是在學校讀書但學習的東西卻有很大的不同，雖然碩班學習的內容只是化學領域中小小的分支，但由於周必泰老師具有淵博學識、又精通各種領域，使我學習到的東西不僅僅只有光譜，還有各種其它光學相關領域，真的非常感謝周老師的教導，教導我們如何將課本上的知識應用於實驗上，使我從一個完全不懂光譜的學生能夠漸入佳境。

這兩年除了非常感謝指導教授周必泰 教授的教導之外，也要感謝帶領我進入光譜實驗的郭廷逸學長，還有感謝教導我飛秒實驗的唐國鈞學長及何志偉學長，以及幫助我計算光譜性質的潘校安學長、劉士弘學長及陳其霖學長，最後還要感謝辛苦合成化合物的黃懷慶學長、沈俊義學長及張志雲學長，以及感謝實驗室其他學長姐的幫忙與教導像陳協志學長、陳怡安學姊、陳英校學長、張育佳學姊...。

感謝實驗室學長姐學弟妹及我親愛的同學這兩年的陪伴，使我的碩班生活多采多姿，每天除了實驗之外還發生許多有趣的事。

謝謝子胤每天跟我聊生活大小事，還讓我假日有地方可以玩，還有謝謝新竹同學們的邀約，讓我的假期生活更豐富，謝謝芸瑄學姐在我碩一剛進台大時，常關心我還騎腳踏車載我上學，還有謝謝珮聰每個禮拜的運動邀約雖然常常互相放鴿子 XDDD。

最後要感謝我的家人，謝謝父母辛苦賺錢讓我碩班生活不愁吃穿，謝謝我的姊姊跟弟弟當我不在家的時候陪伴爸媽，還有謝謝我妹常來台北找我住，希望接下來一切順利~

謝謝在我生命中出現的每個人~不管是好是壞，都使我更茁壯更豐富了我的經歷
希望大家平安快樂~~



中文摘要

水催化 7-azaindole (**7AI**) 進行激發態質子轉移的機制已經長期被研究但其結論具有爭議性。由於最近成功的使用 7-azaindole (**7AI**) 相似物 2,7-diazatryptophan 來偵測蛋白質周圍的水分子，因此我們再回去研究 **7AI** 及其相似物之水催化激發態質子轉移的機制，並將過去的論點及目前的結果整合整理出更合理的機制。藉由合成一系列 **7AI** 相似物及其甲基化衍生物，並具有系統性的研究 pK_a ， pK_a^* 以及相關的螢光光譜及動力學探討。從量測出來的結果，我們認為所有 **7AI** 衍生物在中性的水中都會經由水的催化進行激發態質子轉移。然而對於在三號位接推電子基(包括氫)的衍生物經由水催化進行激發態質子轉移形成激發態互變異構體(T^*)，此互變異構體迅速發生質子化產生激發態陽離子，再經由快速的去活化過程回到標準態(N)形式的基態。相反的，對於在二號或三號位接拉電子基或二號位的碳原子被拉電子性較強的氮原子取代的衍生物(2,7-diazatryptophan)其激發態互變異構體(T^*)不會進行質子化形成陽離子，而會以激發態互變異構體(T^*)形式產生綠色的放光。同時藉由合成相關的 $N(7)-CH_3$ 異構體形式的分子來作為補充支持我們的論點，對於其陽離子形式($N(7)-CH_3N(1)-H^+$)的 pK_a^* 值，如果是三號位接推電子基其值大於 7，而接拉電子基則小於 7。**7AI** 之前於 pH 7-12 之間看不見互變異構體(T^*)的放光,但現在於 pH 13.0 - 14.5 之間可以很清楚的解析出放光峰在波長 530nm 互變異構體(T^*)的放光。

關鍵字: 7-azaindole， pK_a ， pK_a^* ，激發態質子轉移(ESPT)，互變異構體



Abstract

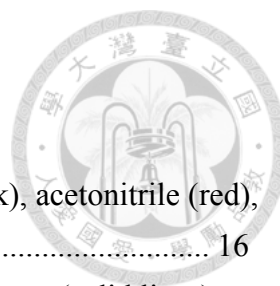
The mechanism of water-catalyzed excited-state proton transfer (ESPT) reaction for 7-azaindole (**7AI**) has long been investigated, but there are some controversial viewpoints. Recently, owing to the superiority of sensing biowaters in proteins by a **7AI** analogue, 2,7-diazatryptophan, it is timely to reinvestigate water-catalyzed ESPT in **7AI** and its analogues in an attempt to unify the mechanism. Herein, a series of **7AI** analogues and their methylated derivatives were synthesized to carry out a systematic study on pK_a , pK_a^* and the associated fluorescence spectroscopy and dynamics. The results conclude that all **7AI** derivatives undergo water catalyzed ESPT in neutral water. However, for those derivatives with electron-donating substituent (including -H) at C(3), following water catalyzed ESPT to form an excited N(7)-H proton-transfer tautomer, T^* , rapid protonation takes place to generate an excited cationic (TC^*) species that subsequently undergoes a fast deactivation to the N(1)-H normal species in the ground state. Conversely, protonation in T^* is prohibited for those derivatives with an electron-withdrawing groups at the C(2) or C(3), or C(2) atom replaced by an electron-withdrawing nitrogen atom (N(2) in e.g., 2,7-diazatryptophan), giving a prominent green T^* emission. Additional support is given by the synthesis of the corresponding N(7)-CH₃ tautomer species, for which pK_a^* of the cationic form, i.e., the N(7)-CH₃N(1)-H⁺ species, is measured to be much greater than 7.0 for those with electron-donating C(3) substituents, whereas it is lower than 7.0 upon anchoring electron-withdrawing groups. For **7AI** the previously missing T^* emission is clearly resolved with peak wavelength at 530 nm in the pH interval of 13.0-14.5.

keywords: 7-azaindole, pK_a , pK_a^* , excited-state proton transfer (ESPT), tautomer

Contents



謝辭	I
中文摘要	II
Abstract	III
Contents	IV
List of Figures	V
List of Tables	VII
List of Schemes	VIII
1. Introduction	1
2. Experimental Section	7
2.1 Materials	7
2.2 Spectroscopic Measurements	12
2.3 Computational Methodology	14
3. Results and Discussion	15
4. Conclusion	39
5. References	41
6. Supporting Information	47



List of Figures

- Figure 1.** Steady state emission spectra of **7AI** in cyclohexane (black), acetonitrile (red), DMSO (green), and water (blue) at room temperature. 16
- Figure 2.** (a) Steady-state absorption (dashed lines) and emission spectra (solid lines) and (b) emission decay kinetic traces for **7AI** in room-temperature water with the presence of different concentrations of Zn^{2+} 18
- Figure 3.** Steady-state absorption (dashed lines) and emission spectra (solid lines) for **7AI** in water at indicated pH values at room temperature. 22
- Figure 4.** Steady-state absorption spectra (dashed lines) and emission spectra (solid lines) for **7AI** (black and blue) and **7M7AI** (green) in water at room temperature. The pH values of the solutions are indicated in the figure..... 22
- Figure 5.** Normalized excitation spectra for 7-azaindole (**7AI**) in a room-temperature aqueous solution monitored at the normal emission band (400 nm, blue curve) and the tautomer emission band (550 nm, green curve). The concentration of NaOH is 1.96 M and the pH is 14.3. A normalized absorption spectrum of **7AI** is also included for comparison (red curve). 23
- Figure 6.** Femtosecond fluorescence up-conversion kinetic traces for the normal form emission (430 nm) and tautomer emission (580 nm) of **7AI** in the $\text{NaOH}_{(\text{aq})}$ solution (pH 14) at room temperature. The excitation wavelength is 268 nm..... 25
- Figure 7.** Steady state emission spectrum for 4-azaindole (**4AI**) in an $\text{NaOH}_{(\text{aq})}$ solution (pH 14.3) at room temperature. 26
- Figure 8.** Femtosecond fluorescence up-conversion dynamics of **7AI** monitoring at 420 nm, 470 nm and 500 nm in neutral water at room temperature. The excitation wavelength is 268 nm..... 28
- Figure 9.** Steady-state absorption (dashed lines) and emission spectra (solid lines) for **7AI** (blue), **3MAI** (black), **2CF₃AI** (green), **3CAI** (red) in neutral water at room temperature. 33
- Figure 10. (a)** The proposed water catalyzed ESPT for **7AI** derivatives. **(b)** The mechanism of water catalyzed ESPT and the following deactivation pathways for **7AI** derivatives in the neutral water. The asterisk * indicates the electronic excited state. 37
- Figure 11.** The proposed deactivation pathway of the proton-transfer tautomer cation in the excited state. The asterisk * denotes the electronic excited state. 38
- Figure S1.** Spectral data analysis and $\text{p}K_{\text{a}}$ determination. (a) Steady-state absorption

spectrum of 3MAI in different pH value. (b) Plot of the absorbance of 355 nm vs. pH to determine the pK_a	49
Figure S2. Spectral data analysis and pK_a^* determination. (a) Steady-state emission spectrum of 3MAI in different pH value with 285 nm excitation. (b) Plot of the emission intensity of 375 nm vs. pH to determine the pK_a^*	50
Figure S3. Spectral data analysis and pK_a determination. (a) Steady-state absorption spectrum of 7M3MAI in different pH value. (b) Plot of the absorbance of 395 nm vs. pH to determine the pK_a	51
Figure S4. Spectral data analysis and pK_a^* determination. (a) Steady-state emission spectrum of 7M3MAI in different pH value with 350 nm excitation. (b) Plot of the emission intensity of 550 nm vs. pH to determine the pK_a^*	52
Figure S5. Spectral data analysis and pK_a determination. (a) Steady-state absorption spectrum of 7M(2,7-aza)Trp in different pH value. (b) Plot of the absorbance of 405 nm vs. pH to determine the pK_a	53
Figure S6. Spectral data analysis and pK_a^* determination. (a) Steady-state emission spectrum of 7M(2,7-aza)Trp in different pH value with 342 nm excitation. (b) Plot of the emission intensity of 400 nm vs. pH to determine the pK_a^*	54
Figure S7. Spectral data analysis and pK_a determination. (a) Steady-state absorption spectrum of 7M2CF₃AI in different pH value. (b) Plot of the absorbance of 360 nm vs. pH to determine the pK_a	55
Figure S8. Spectral data analysis and pK_a^* determination. (a) Steady-state emission spectrum of 7M2CF₃AI in different pH value with 315 nm excitation. (b) Plot of the emission intensity of 500 nm vs. pH to determine the pK_a^*	56



List of Tables

Table 1. Emission quantum yields (Φ_{em}) and observed emission lifetimes (τ_{obs}) for 7AI in room-temperature water with the presence of different concentrations of Zn^{2+} . 17	
Table 2. Ground- and excited-state pK_a for the protonated form of 7AI, 3MAI and various 7AI methyl (N(7)- CH_3) tautomer analogues (See Scheme 1 for their structures)..... 19	19
Table 3. The calculation of electron density distribution of N(1) and N(7) atoms in water for 7AI and its analogues (See Scheme 1 for their structures). 29	29



List of Schemes

Scheme 1. Chemical structures of various 7AI derivatives and their methyl (N(7)-CH ₃) tautomer. analogues.....	1
Scheme 2. Chemical structures of 4-azaindole (4AI).....	25




1. Introduction

Excited-state proton transfer (ESPT) reactions have attracted considerable attention due to their occurrence in a wide variety of photophysical and photochemical processes.

The mechanism of ESPT, which correlates with the strength of a hydrogen bond (H-bond) and dynamics of proton (or hydrogen atom) motion, provides valuable information on the fundamental of chemical reaction as well as mimicking proton-transfer processes that ubiquitously take place in biological systems.

Scheme 1. Chemical structures of various **7AI** derivatives and their methyl (N(7)-CH₃) tautomer. analogues.

	R ₁	R ₂	R ₃	Compound
	H	C	H	7AI
	CH ₃	C	H	3MAI
	CH ₂ CHNH ₂ CO ₂ H	N	—	(2,7-aza)Trp
	CN	C	H	3CAI
	H	C	CF ₃	2CF₃AI
	R ₁	R ₂	R ₃	Compound
	H	C	H	7M7AI
	CH ₃	C	H	7M3MAI
	CH ₂ CHNH ₂ CO ₂ H	N	—	7M(2,7-aza)Trp
	CN	C	H	7M3CAI
	H	C	CF ₃	7M2CF₃AI



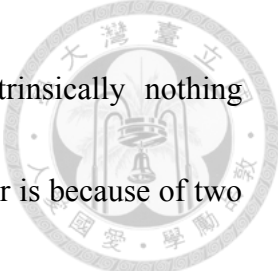
Among numerous ESPT molecules, 7-azaindole (**7AI**, see **Scheme 1**) has shown its photophysical uniqueness and hence great bio-significance. Azaindole is analogous to indole that forms the base of amino acid tryptophan and is akin to the adenine nucleobase. The photophysics of **7AI** have been widely investigated in a variety of environments. In hydrocarbon solvents, Kasha and co-workers first demonstrated that in concentrated solution **7AI** formed dual H-bond dimers, which upon electronic excitation undergo excited-state double proton transfer (ESDPT)¹ to give a green proton-transfer tautomer emission. In this regard, the **7AI** doubly hydrogen bonded dimer with its ESDPT has long been served as a prototype to illustrate the possible photoinduced proton transfer taking place in the DNA double helix and consequently the cause of mutation.²⁻⁴

The excited-state tautomerization also proceeds efficiently in protic solvents such as alcohols. The ESDPT process in alcohol has been explained in terms of a two-step model,⁵⁻⁷ in which the formation of **7AI**-solvent molecule cyclic H-bond complex is the prerequisite and rate-determining step, followed by the fast proton tunneling process. The rate of tautomerization reaction typically requires several hundred picoseconds,

which is two orders of magnitude slower than the reaction rate for its dual hydrogen-bonding dimer in hydrocarbon solvents.^{8,9}




The photophysical behavior of **7AI** in water, however, appeared to be anomalous. In sharp contrast to the dual emission bands for **7AI** in alcohols, consisting of two well-separated normal (~370 nm, N*) and proton transfer tautomer (~510 nm, T*) bands, only a single band maximized at ~385 nm is resolved in neutral water. Several research groups have studied the emission of **7AI** in water and reached different conclusions regarding its origin and hence different mechanisms. On the one hand, Petrich and co-workers⁶ interpreted the photophysics of **7AI** in water by proposing that only a small fraction (< 20%) of the **7AI** molecules in pure water are capable of undergoing excited-state tautomerization on a 1 ns time scale. No appreciable emission intensity can be observed for **7AI** in water at around 530 nm because very little tautomer is generated and is rapidly protonated to give a tautomer cationic emission (~440 nm) that is buried under the major normal (385 nm) emission. On the other hand, Chapman and Maroncelli also carefully analyzed the relaxation dynamics of **7AI** in water and came up with somewhat different viewpoints.¹⁰ They concluded that even though the emission spectra for **7AI** in alcohols (dual emission) and water (single



emission band) appear to be qualitatively different, there is intrinsically nothing anomalous about the behavior of **7AI** in water. The spectral dissimilar is because of two quantitative differences in terms of rates. In water, while the rate of $N^* \rightarrow T^*$ proton transfer is much slower, the nonradiative deactivation for T^* is very fast. The combination of these two effects leads to a consequence of only normal (N^*) emission band being observed.

In yet another approach in chemical biology, 7-azatryptophan, an analogue of **7AI**, has long been applied as an alternative of tryptophan to probe the protein structure and dynamics.¹¹⁻¹³ This is mainly due to the fact that 7-azatryptophan possesses both longer absorption spectral onset (cf. tryptophan) and polarity-sensitive emission peak wavelength. Unfortunately, similar to that of **7AI**, 7-azatryptophan in water lacks proton-transfer tautomer emission and could not be used as a marker to probe the surrounding water environment in proteins. In proteins, water ubiquitously participates in dictating structure and functionality. Recent advances have provided more convincing evidence that water molecules in proteins are one of the key elements in activating bio-functionalities such as enzymatic reactions.¹⁴⁻¹⁷



In an aim to specifically probe water environment, we recently replaced C(2) of 7-azatryptophan (see **Scheme 1** for numbering) by a nitrogen atom (N(2)), forming 2,7-diazatryptophan (**(2,7-aza)Trp**) that exhibits remarkable water-catalyzed proton-transfer properties.¹⁸ **(2,7-aza)Trp** exists in two isomers in the ground state, i.e., the N(1)-H and N(2)-H isomers, in which the N(1)-H isomer undergoes water-catalyzed ESPT, resulting in an N(7)-H tautomer emission maximized at 500 nm. This prominent proton-transfer emission thus serves as a unique fingerprint and has been successfully exploited for direct sensing of a site-specific water environment in the human thromboxane A2 synthase (hTXAS) without disrupting its native structure.¹⁸ We also noticed that upon removing the α -amino acid part from **(2,7-aza)Trp**, forming 2,7-diazaindole, similar proton transfer emission was also resolved, which is in stark contrast to the lack of tautomer emission for **7AI** in water. From the fundamental point of view, a core issue is thus raised regarding factors that govern the water catalyzed ESPT and hence the resolution of proton-transfer tautomer emission. This, together with the long-standing puzzle regarding mechanism of ESPT for **7AI** in water, leads us to revisit water catalyzed excited-state proton transfer in **7AI**. We also carried out a systematic study on pK_a , pK_a^* and the associated fluorescence spectroscopy/dynamics

for a series of **7AI** derivatives and their methylated tautomer analogues. The results conclude that the luminescence properties are harnessed by the excited-state acidity/basicity properties of the proton-transfer tautomer and the overall ESPT mechanism in water can be unified among the titled **7AI** derivatives. Detail of results and discussion is elaborated as follows.





2. Experimental Section

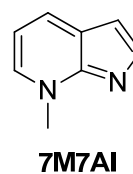
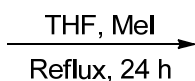
2.1 Materials.

Azaindole precursors and other reagents were commercially available and were used without further purification. All solvents were purchased from Acros and Merck. Silica gels were from Merck (230-400 mesh).

Syntheses and Characterizations.

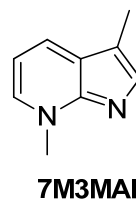
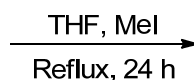
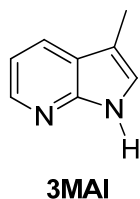
General Procedure for the Synthesis of the methyl (N(7)-CH₃) tautomer compounds.

The corresponding azaindole (1 eq.) and MeI (3 eq.) were dissolved in THF into a sealed bottle, then the mixture was heated to reflux for 24 h. After cooling, the solid was formed and filtered. Then, the solid was dissolved in water and washed three times with dichloromethane. The aqueous solution was adjusted pH to 12 with NaOH_(aq) and extracted by dichloromethane. The organic layer was dried over MgSO₄ and filtered. The organic layer was evaporation under reduced pressure and dried under vacuum. The methyl (N(7)-CH₃) tautomer compound was obtained without further purification.



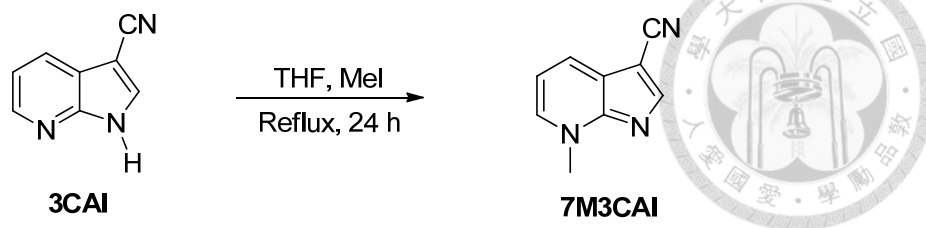
7-methyl-7H-pyrrolo[2,3-b]pyridine (7M7AI) : Follow the general procedure.

Yield: 38%. ^1H NMR (400 MHz, CDCl_3): δ 4.17 (s, 3H), 6.60 (d, $J = 2.4$ Hz, 1H), 6.72 (t, $J = 7.2$ Hz, 1H), 7.43 (d, $J = 6.0$ Hz, 1H), 7.82 (d, $J = 2.4$ Hz, 1H), 8.02 (d, $J = 7.2$ Hz, 1H). ^{13}C NMR (100 MHz, CDCl_3): δ 39.7, 101.0, 108.5, 129.5, 129.6, 130.2, 144.7, 148.5. FAB MS (m/z): 133 ($\text{M}+\text{H}$) $^+$.

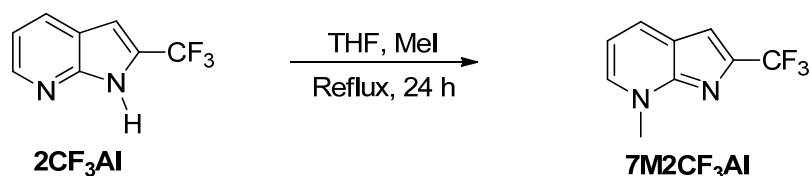


3,7-dimethyl-7H-pyrrolo[2,3-b]pyridine (7M3MAI) : Follow the general procedure.

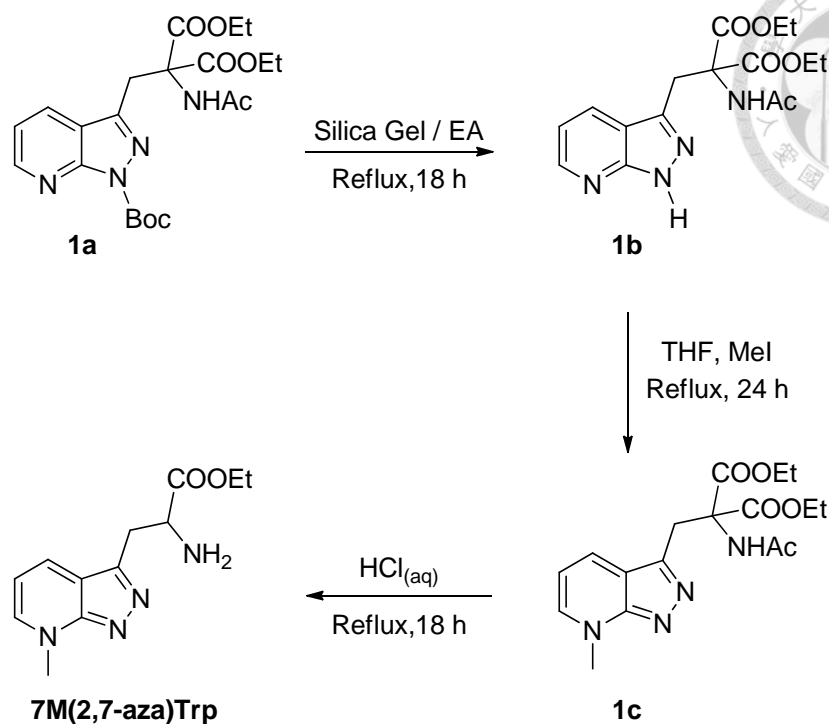
Yield: 45%. ^1H NMR (400 MHz, CDCl_3): δ 2.35 (s, 3H), 4.24 (s, 3H), 6.78-6.82 (m, 1H), 7.52 (d, $J = 6.0$ Hz, 1H), 7.60 (s, 1H), 7.98 (d, $J = 7.2$ Hz, 1H). ^{13}C NMR (100 MHz, CDCl_3): δ 9.6, 39.9, 107.9, 110.7, 128.7, 129.5, 130.2, 142.8, 148.6. FAB MS (m/z): 147 ($\text{M}+\text{H}$) $^+$.



7-methyl-7H-pyrrolo[2,3-b]pyridine-3-carbonitrile (7M3CAI) : Follow the general procedure. Yield: 32%. ^1H NMR (400 MHz, CDCl_3): δ 4.33 (s, 3H), 7.07-7.10 (m, 1H), 7.78 (d, $J = 5.6$ Hz, 1H), 8.21 (s, 1H), 8.24 (d, $J = 7.6$ Hz, 1H). ^{13}C NMR (100 MHz, CDCl_3): δ 40.7, 84.9, 112.1, 116.6, 129.6, 131.6, 132.3, 148.8, 152.3. FAB MS (m/z): 158 (M+H) $^+$.



7-methyl-2-(trifluoromethyl)-7H-pyrrolo[2,3-b]pyridine (7M2CF₃AI): Follow the general procedure. Yield: 30%. ^1H NMR (400 MHz, CDCl_3): δ 4.31(s, 3H), 6.93-6.96 (m, 2H), 7.72 (d, $J = 6.0$ Hz, 1H), 8.22 (d, $J = 7.6$ Hz, 1H). ^{13}C NMR (100 MHz, CDCl_3): δ 40.2, 100.5, 110.1, 121.5, 124.1, 128.5, 132.8, 134.1, 147.9. FAB MS (m/z): 201 (M+H) $^+$.



Diethyl-2-((1*H*-pyrazolo[3,4-*b*]pyridin-3-yl)methyl)-2-acetamidomalonate (1b**).**

Compound **1a** (1 g) was dissolved in ethyl acetate and silica gel (50 g) was added and refluxed for 18h. The solution was allowed to cool down to room temperature. The silica gel in the solution was filtered and washed using ethyl acetate (5 × 100 mL). The filtrate was evaporated under reduced pressure and **1b** was obtained as a white solid. Yield: 90%. ¹H NMR (400 MHz, CDCl₃): δ 1.27 (t, *J* = 7.2 Hz, 6H), 1.88 (s, 3H), 4.05 (s, 2H), 4.23-4.32 (m, 4H), 6.70 (s, 1H), 7.11 (dd, *J* = 8.0, 4.4 Hz, 1H), 7.98 (d, *J* = 8.0 Hz, 1H), 8.51 (d, *J* = 4.4 Hz, 1H), 11.2 (s, 1H). ¹³C NMR (100 MHz, CDCl₃): δ 13.9,

22.9, 30.0, 62.8, 66.4, 115.6, 116.6, 129.5, 140.5, 148.7, 151.9, 167.4, 169.5. FAB MS

(m/z): 349 (M+H)⁺.



Diethyl-2-acetamido-2-((7-methyl-7H-pyrazolo[3,4-b]pyridin-3-yl)methyl)mal

onate (1c). Follow the general procedure. Yield: 15 %. ¹H NMR (400 MHz, CDCl₃): δ

1.26 (t, *J* = 7.2 Hz, 6H), 1.87 (s, 3H), 4.08 (s, 2H), 4.27 (q, *J* = 7.2 Hz, 4H), 4.33 (s, 3H),

6.87-6.90 (m, 1H), 6.96 (s, 1H), 7.79 (d, *J* = 6.8 Hz, 1H), 8.24 (d, *J* = 7.6 Hz, 1H). ¹³C

NMR (100 MHz, CDCl₃): δ 13.7, 22.8, 30.3, 40.3, 62.4, 66.4, 109.3, 123.2, 134.7, 136.1,

143.4, 150.2, 167.4, 169.3. FAB MS (m/z): 363 (M+H)⁺.

2-amino-3-(7-methyl-7H-pyrazolo[3,4-b]pyridin-3-yl) propanoic acid

(7M(2,7-aza)Trp): Compound **3c** (0.89 g, 2.0 mmol) was dissolved in 12 M HCl and

heated to reflux for 8 h. The reaction mixture was concentrated under reduced pressure

to afford **7M(2,7-aza)Trp** as a white solid in the HCl salt form. ¹H NMR (400 MHz,

D₂O): δ 3.85 (d, *J* = 6.0 Hz, 2H), 4.44 (s, 3H), 4.68 (t, *J* = 6.0 Hz, 1H), 7.68-7.71 (m,

1H), 8.81 (d, *J* = 6.0 Hz, 1H), 8.98 (d, *J* = 8.0 Hz, 1H). ¹³C NMR (100 MHz, D₂O): δ

26.6, 42.6, 51.6, 117.7, 120.2, 140.9, 142.4, 144.6, 145.4, 170.5. FAB MS (m/z): 221

(M+H)⁺.

2.2 Spectroscopic Measurements.



Steady-state absorption and emission spectra were recorded with a Hitachi (U-3310) spectrophotometer and an Edinburgh (FS920) fluorometer, respectively. The relative quantum yield measurement is used in the experiment. Quinine sulfate in 0.1M H₂SO₄, with a quantum yields of 0.57 respectively, were used as the standards for the quantum yield measurements. The equation 1 is used to calculate the relative quantum yield.

$$Q = Q_R \frac{I}{I_R} \frac{OD_R(\lambda)}{OD(\lambda)} \frac{n^2}{n^2_R} \quad (\text{Eq. 1})$$

Q: quantum yield

I: integrated area under the corrected emission spectrum

OD: optical density

n: refractive index of the solution

Subscript R: standard of quinine sulfate

Detailed time-resolved spectroscopic measurements were reported previously.^{19,20} In brief, nanosecond time-resolved studies were performed by using an Edinburgh FL 900 time-correlated single photon-counting (TCSPC) system with a pulsed hydrogen filled lamp as the excitation light source. The pulse frequency is 40 kHz. Data were fitted with

sum of exponential functions using the nonlinear least-squares procedure in combination with the convolution method.



Ultrafast spectroscopic study were performed by a femtosecond fluorescence up-conversion system (FOG100, CDP) pumped by the femtosecond oscillator (Tsunami, Spectra-Physics) with central output wavelength at 805 nm. In this measurement, fluorescence from a rotating sample cell, following the excitation at 268 nm (THG of 805 nm), was collected, focused, and frequency summed in a BBO crystal, along with an interrogation gate pulse at designated delay time with respect to the pump pulse. A $\lambda/2$ waveplate was used to set the pump polarization at the magic angle (54.7°) with respect to gate pulse for preventing the fluorescence anisotropy contributed by solute reorientation. Fluorescence up-conversion data were fitted to the sum of exponential functions convoluted with the instrument response function (IRF). The IRF was determined from the Raman scattering signal and its profile was fitted to a Gaussian function with full width at half maximum of ~ 150 fs.

2.3 Computational Methodology.

For all title molecules, the geometries of the ground state were optimized by the density functional theory (DFT) method, and excited state structure with related photophysical properties were calculated by time-dependent density functional theory (TD-DFT) method with B3LYP hybrid function. The 6-31+G(d,p) basis set were employed for all atoms. All theoretical calculations were performed using Gaussian 09 program.²¹



3. Results and Discussion



The related evidence supports of ESPT for 7AI in water

In the early approach, El-Bayoumi *et al.* compared the isotope effect and emission quantum yield of 7AI with indole and N₁-methyl-7-azaindole in H₂O.²² They found that 7AI had a relatively low emission quantum yield of 0.03 in H₂O and a relatively large isotope effect ($\Phi_{\text{D}_2\text{O}}/\Phi_{\text{H}_2\text{O}} = 3.63$). They concluded that both the N(7) and N(1)-H sites were involved in the deactivation process. In addition, Chapman and Maroncelli observed nearly identical radiative decay rate constants for 7AI in H₂O ($3.7 \times 10^7 \text{ s}^{-1}$) and in D₂O ($3.6 \times 10^7 \text{ s}^{-1}$), but a larger non-radiative decay rate constant in H₂O ($1.2 \times 10^9 \text{ s}^{-1}$) than in D₂O ($2.9 \times 10^8 \text{ s}^{-1}$).¹⁰ To probe the water catalytic effect on 7AI, in an early approach, Chou and co-workers gradually added a small amount of water into the aprotic solvent containing 7AI and observed the growth of green proton-transfer tautomer emission. The result clearly proves that water molecules are capable of catalyzing the proton transfer reaction for 7AI in the excited state.²³ Based on these observations, one would speculate that the quenching pathway of 7AI in water is highly related to excited-state water-catalyzed ESPT that is subject to the deuterium isotope effect.

The emission spectrum of **7AI** is sensitive and can be red-shifted by increasing solvent polarity (**Figure 1**). The emission maximum of **7AI** is 310 nm in cyclohexane and 385 nm in pure water. Although there is only a small difference in the normal form emission maximum of **7AI** in DMSO (360 nm) and water (385 nm), the emission quantum yields and lifetimes are drastically different, being as high as 0.36 (Φ_{em}) and 9.2 ns (τ_{obs}) in DMSO but as small as 0.03 (Φ_{em}) and 0.9 ns (τ_{obs}) in water.

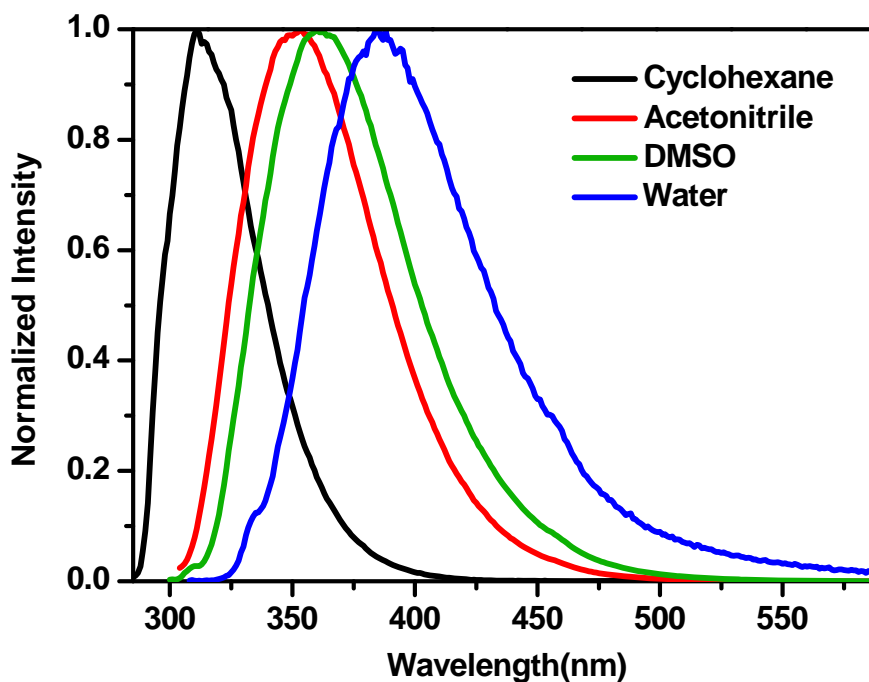
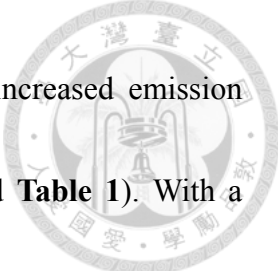


Figure 1. Steady state emission spectra of **7AI** in cyclohexane (black), acetonitrile (red), DMSO (green), and water (blue) at room temperature.

In order to understand whether the much smaller emission quantum yield and shorter lifetime in water are due to ESPT, Zn^{2+} (in the form of $ZnCl_{2(aq)}$) is added to the



solution to coordinate with **7AI** at the N₁ and N₇ positions and increased emission quantum yields and extended lifetimes are observed (**Figure 2** and **Table 1**). With a Zn²⁺ concentration of 0.02 M, the Φ_{em} increases from 0.03 to 0.09 and the emission decay kinetic trace shows two lifetimes: 0.9 ns for free (un-coordinated) **7AI** and 26.1 ns for Zn²⁺-coordinated **7AI**. When the concentration of Zn²⁺ is increased to 0.5 M, the Φ_{em} increases to 0.5 and one emission decay lifetime of 18.4 ns is measured. The high Φ_{em} and long lifetime for Zn²⁺-coordinated **7AI** are close to those for N₁-methyl-7-azaindole (**1M7AI**) (Φ_{em} = 0.54 and τ = 26 ns in water).¹⁰ These results strongly suggest that ESPT is the major excited-state deactivation pathway for **7AI** in water.

Table 1. Emission quantum yields (Φ_{em}) and observed emission lifetimes (τ_{obs}) for **7AI** in room-temperature water with the presence of different concentrations of Zn²⁺.

[Zn²⁺] / M	Φ_{em}	τ_{obs} / ns (% of pre-exp factors)
0.02	0.09	0.9 (96 %); 26.1 (4 %)
0.10	0.24	0.9 (83 %); 23.1 (17 %)
0.25	0.38	0.9 (59 %); 20.6 (41 %)
0.50	0.50	18.4 (100 %)

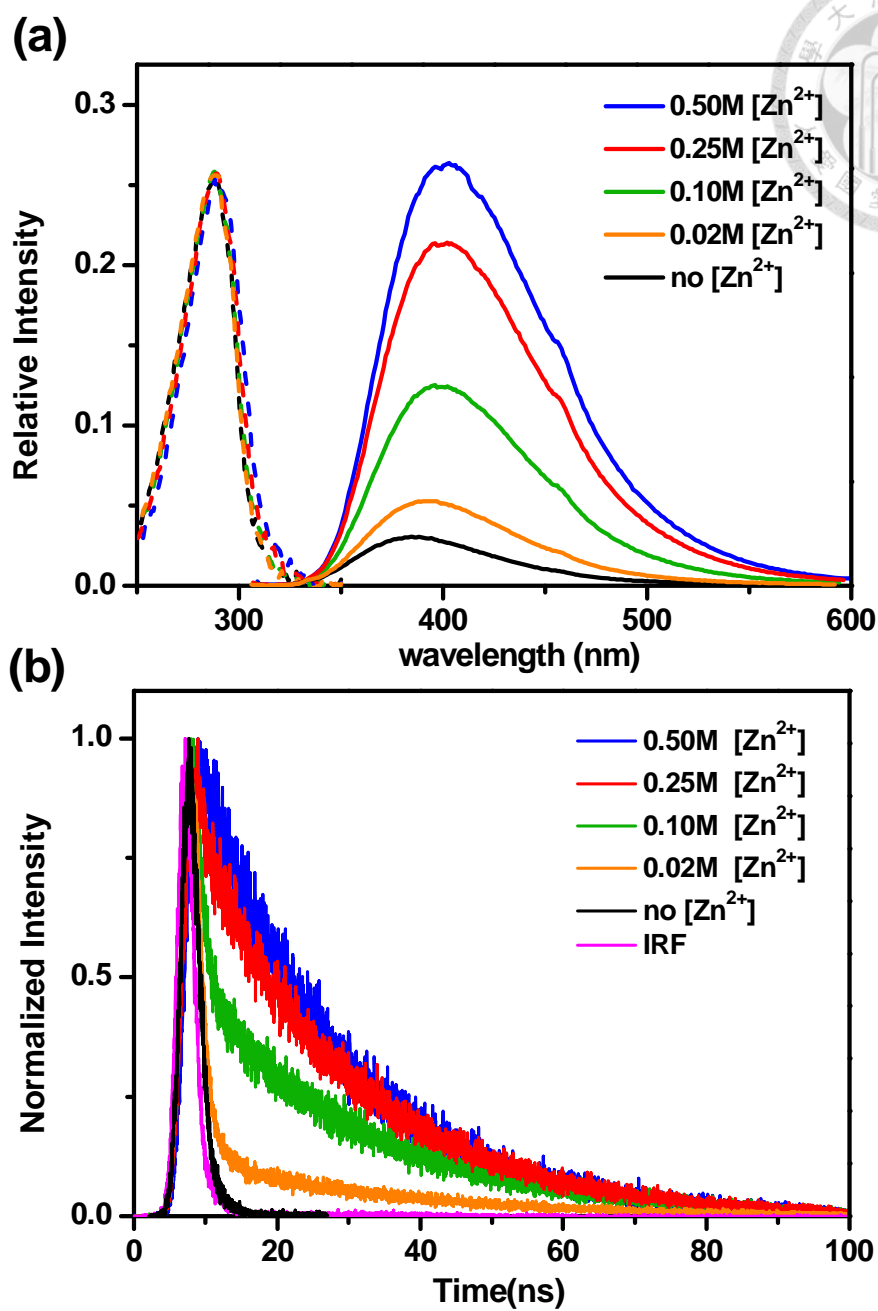


Figure 2. (a) Steady-state absorption (dashed lines) and emission spectra (solid lines) and (b) emission decay kinetic traces for **7AI** in room-temperature water with the presence of different concentrations of Zn^{2+} .




The direct evidence supports of ESPT for 7AI in water

Despite a number of relevant supports of ESPT for 7AI in water, the direct support of ESPT, i.e. the observation of tautomer emission, is unfortunately missing (vide supra).

The pK_a^* of 7AI tautomer analogue 7-methyl-7H-pyrrolo[2,3-b]pyridine (7M7AI) (see **Table 2** and **Scheme 1**) in protonated form 7M7AI was measured to be 10.3.⁶ Assuming similar pK_a^* between 7M7AI cation (N(1)-H⁺) and the protonated 7AI tautomer (N(1)-H⁺), Petrich and co-worker thus proposed that 7AI tautomer should be in the protonated form at pH 7. In other words, the 7AI tautomer in the excited state, once being produced from water catalyzed ESPT, is promptly protonated in the neutral water so that the tautomer emission is absent.

Table 2. Ground- and excited-state pK_a for the protonated form of 7AI, 3MAI and various 7AI methyl (N(7)-CH₃) tautomer analogues (See **Scheme 1** for their structures).

Compound	pK_a	pK_a^*
7AI	4.5 ⁶	4.6 ⁶
3MAI	4.8 ^a	4.6 ^b
7M7AI	8.9 ²⁴	10.3 ⁶
7M3MAI ²⁵	9.3 ^a	9.4 ^c
7M(2,7-aza)Trp	5.8 ^a	5.8 ^d
7M3CAI ²⁶	4.8	0.2
7M2CF ₃ AI	4.4 ^a	-0.3 ^e



^a. Determined by the half-neutralization method. ^b. The excitation wavelength was 285 nm and the emission was monitored at 375 nm for the emission intensity titration experiment. ^c. The excitation wavelength was 350 nm and the emission was monitored at 550 nm for titration. ^d. The excitation wavelength was 342 nm and the emission was monitored at 400 nm for titration. ^e. The excitation wavelength was 315 nm and the emission was monitored at 500 nm for titration.

The above thermodynamic interpretation based on acid-base property to govern the fate of proton transfer emission is sound. However, as for **7AI**, crucial spectroscopic evidences have to be provided to verify the mechanism. First, if the excited N(7)-H tautomer of **7AI** is in the protonated form at pH 7, the associated cationic emission should be resolvable. Second, assuming a similar pK_a^* (10.3) with **7M7AI** cation (N(1)-H⁺) for the protonated **7AI** tautomer (N(1)-H⁺), the neutral N(7)-H tautomer emission should be observable at pH > 10.3; however, no tautomer emission could be resolved up to pH 12. Petrich and co-workers concluded that the lack of both tautomer and tautomer cation emission in neutral water was due to a small (< 20%) portion of **7AI** undergoing water catalyzed ESPT.⁶

Because the **7AI** tautomer emission has not been resolved so far we then suspect

that pK_a^* of protonated **7AI** tautomer (N(1)-H⁺) may be higher than that (10.3) predicted by using **7M7AI** (N(1)-H⁺). We thus extended the fluorescence titration measurement to higher pH value. **Figure 3** clearly shows that in addition to the 385 nm normal emission, the 530 nm N(7)-H tautomer emission gradually appears from pH 13.0 to pH 14.5. The assignment of the tautomer emission can be supported by its spectral feature being nearly identical with the emission spectrum of the tautomer analogue **7M7AI** shown in **Figure 4**. Further support of ESPT is rendered by identical excitation spectra for both the normal and tautomer emission bands, which are also identical with the absorption spectrum (**Figure 5**), indicating that both emission bands share the common ground-state origin.

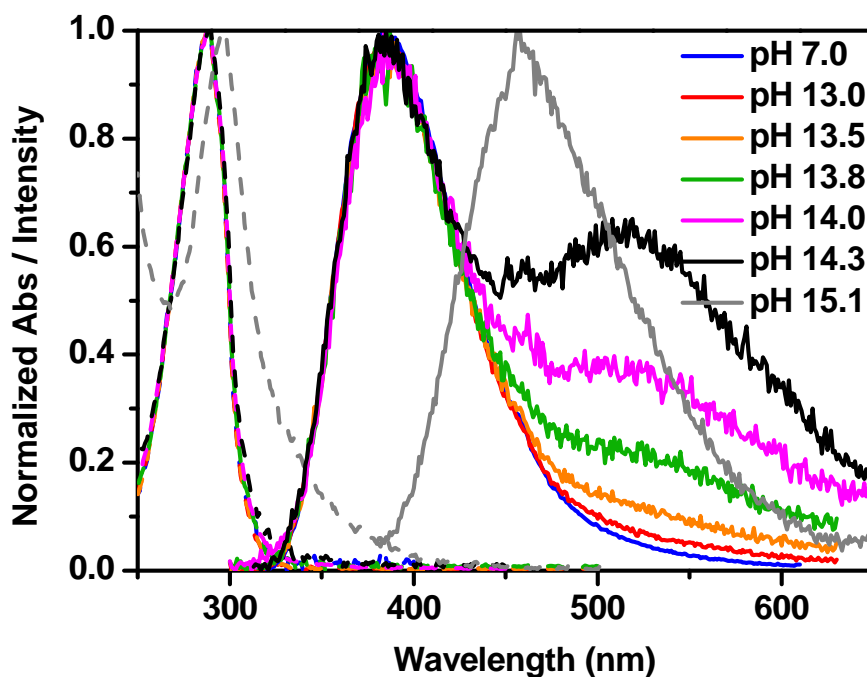




Figure 3. Steady-state absorption (dashed lines) and emission spectra (solid lines) for **7AI** in water at indicated pH values at room temperature.

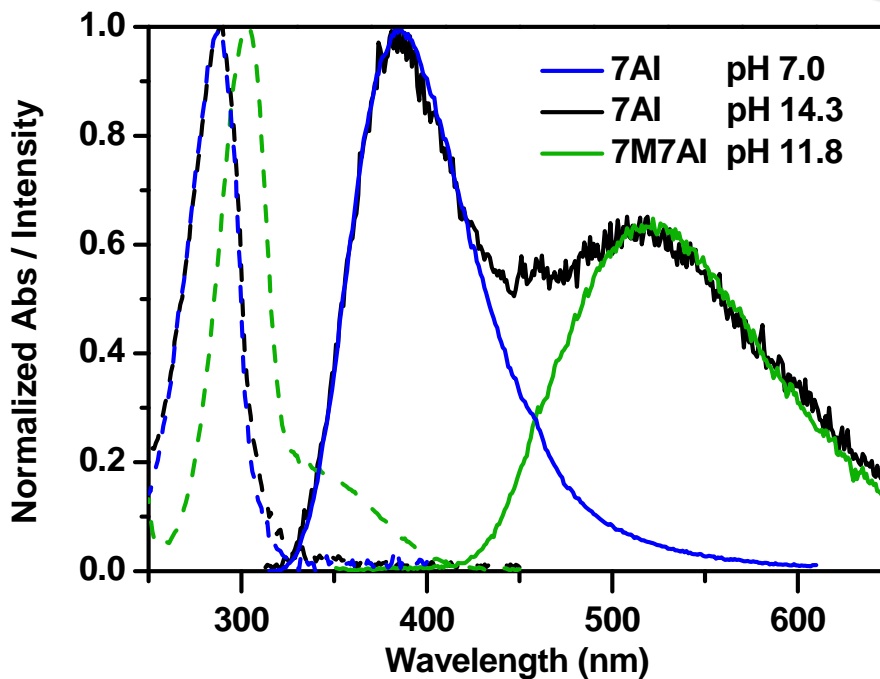


Figure 4. Steady-state absorption spectra (dashed lines) and emission spectra (solid lines) for **7AI** (black and blue) and **7M7AI** (green) in water at room temperature. The pH values of the solutions are indicated in the figure.

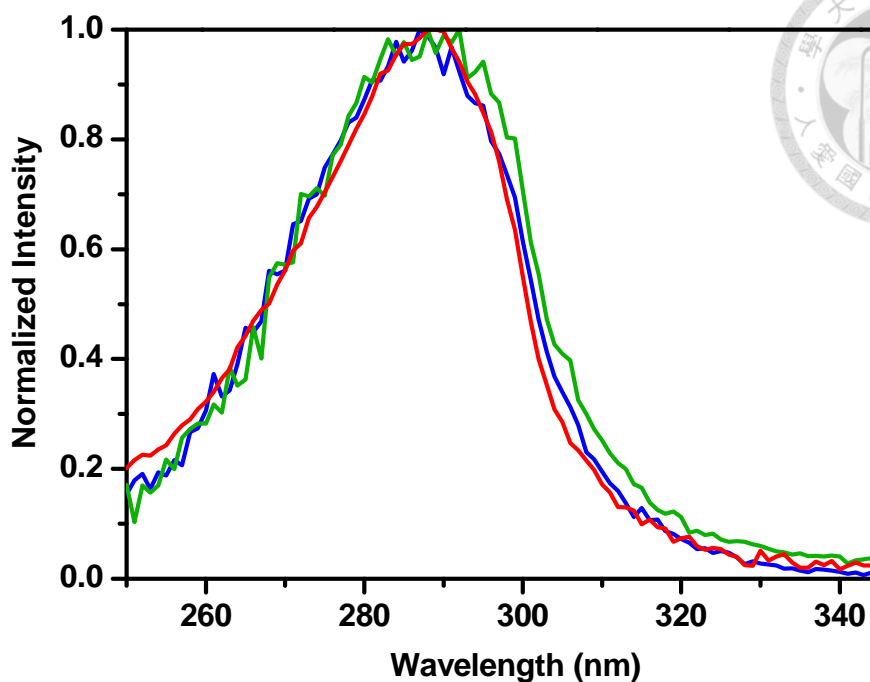
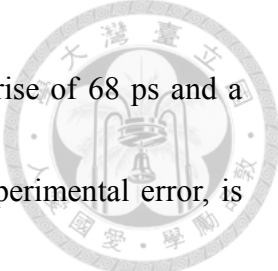


Figure 5. Normalized excitation spectra for 7-azaindole (**7AI**) in a room-temperature aqueous solution monitored at the normal emission band (400 nm, blue curve) and the tautomer emission band (550 nm, green curve). The concentration of NaOH is 1.96 M and the pH is 14.3. A normalized absorption spectrum of **7AI** is also included for comparison (red curve).

Perhaps the firmest support of ESPT is given by the relaxation dynamics of the corresponding emission. At pH 14, the femtosecond fluorescence upconverted signal monitored at normal emission of e.g. 430 nm consists of an instant rise (< 150 fs) and a single exponential decay component with lifetime of 70 ps (**Figure 6**). Upon monitoring at the tautomer emission of 580 nm, the time resolved upconverted signal consists of a



small portion (< 15%) of instant rise component, a relatively slow rise of 68 ps and a population decay time of 190 ps. The rise time of 68 ps, within experimental error, is identical with the decay time (70 ps) of the normal emission, clearly demonstrating the behavior of a precursor-successor type of ESPT reaction. The instant rise component can be rationalized by the certain overlap between the normal and tautomer emissions so that decay (normal emission) and rise (tautomer emission) are cancelled out, causing a net result of instant rise. Under this condition, **7AI** undergoes proton transfer by N(1)-H deprotonation accompanied by the N(7) protonation. The hydrogen-bonded **7AI**/H₂O (1:1) cyclic configuration is not required for proton transfer to happen and the lifetimes observed are much shorter than the 0.9 ns. This argument is also supported by a similar behavior for 4-azaindole (**4AI**) at high pH value.²⁷ A tautomer emission band around 500 nm can be observed for **4AI** at pH 14.3 (**Figure 7**) and since N(1) and N(4) are far away from each other, it is not likely for **4AI** to form a hydrogen-bonded cyclic configuration with a bridge of several water molecules.

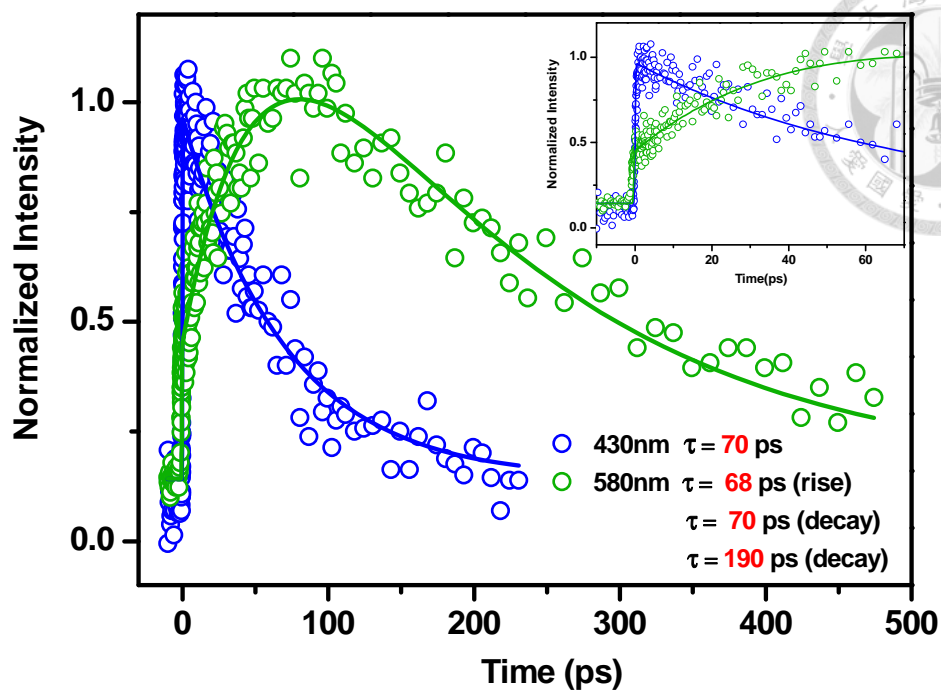
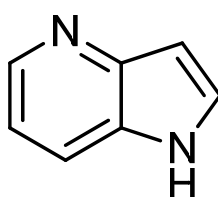


Figure 6. Femtosecond fluorescence up-conversion kinetic traces for the normal form emission (430 nm) and tautomer emission (580 nm) of **7AI** in the $\text{NaOH}_{(\text{aq})}$ solution (pH 14) at room temperature. The excitation wavelength is 268 nm.

Scheme 2. Chemical structures of 4-azaindole (**4AI**).



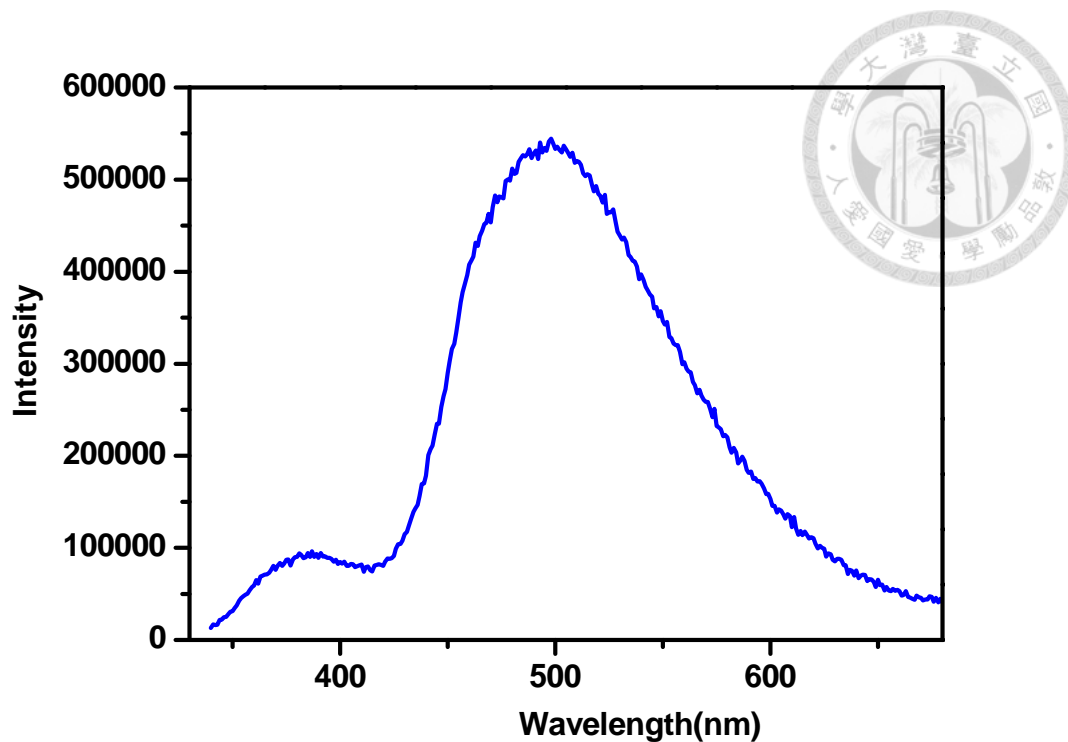



Figure 7. Steady state emission spectrum for 4-azaindole (**4AI**) in an $\text{NaOH}_{(\text{aq})}$ solution (pH 14.3) at room temperature.

Further increasing pH to 15.0 the deprotonation of **7AI** in the ground state takes place, which is clearly indicated by the appearance of an absorption shoulder in the region of 350-400 nm (**Figure 3**), giving rise to a **7AI** anion emission maximized at 465 nm. Therefore, in the steady state measurement the **7AI** tautomer emission can only be resolved in a narrow pH range of ~ 13.0 -14.5, explaining why the **7AI** tautomer was obscure in the previous studies.

In the wake of resolving the **7AI** tautomer emission, another core issue lies in the verification of the tautomer cationic emission in neutral water, which, according to



above proposal, results from the protonation of tautomer in the excited state. The cationic emission of the **7AI** tautomer analogue, i.e., the **7M7AI** ($\text{N}(1)\text{-H}^+$), is around 440 nm.⁶ In neutral water, because **7AI** exhibits solely a 385 nm normal emission band at pH 7 (**Figure 3**), the cationic emission, if existing, must be very weak and associated with a fast non-radiative decay rate. Exploiting the fluorescence upconversion technique, we then made attempts to resolve the tautomer cationic emission of **7AI** in the region of 420-550 nm at pH 7. Upon monitoring the fluorescence upconverted signal at three wavelengths (420, 470 and 500 nm), the corresponding time-resolved profiles all reveal an instant rise (< 150 fs) and a long population decay that remains nearly constant in the region of 50 ps (**Figure 8**). The long decay component is further resolved to be ~ 900 ps, and is unambiguously ascribed to the population decay of the normal **7AI** emission.^{6,10} Thus, under a system response of < 150 fs we were not be able to detect any fast, resolvable component within the emission region of 420-500 nm. On the one hand, this may be rationalized by only a small population of the initial proton-transfer tautomer species in the excited state, as previously proposed by Petrich and co-workers (vide supra). However, because the 530 nm tautomer emission is well resolved within pH 13.0-14.5 in this study, this possibility is discounted. Alternatively, it is more plausible

that the excited tautomer cationic species is an intermediate, which deactivates to normal **7AI** ground state species in a rate faster than its formation. Kinetically, this implies that the population of tautomer cation achieves a steady state and its concentration is thus too small to be resolved. We will elaborate this viewpoint in the following section regarding the generalization of ESPT mechanism for **7AI**.

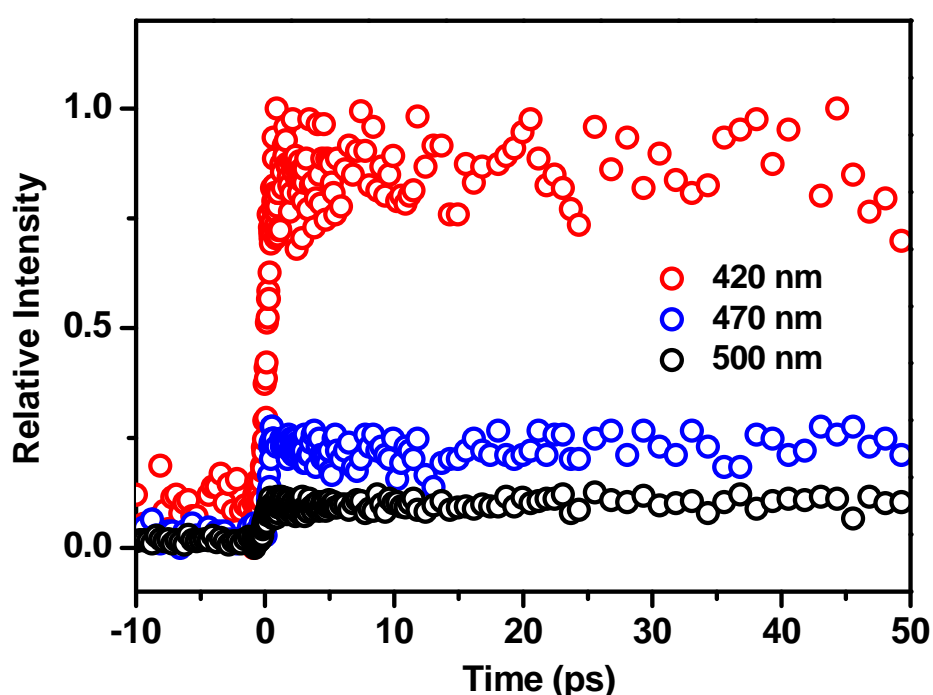


Figure 8. Femtosecond fluorescence up-conversion dynamics of **7AI** monitoring at 420 nm, 470 nm and 500 nm in neutral water at room temperature. The excitation wavelength is 268 nm.

The viewpoint of calculation

To the viewpoint of calculation, upon photo-excitation, electronic charge redistribution is the major driving force for the ESPT reaction in **7AI** and its analogues

to occur and it results in an electron density reduction on the N(1) atom and an increase on N(7) atom (see **Table 3**). Following ESPT, the **7AI** tautomer is expected to have a very different acid-base property when compared with the normal form species. Based on computations, Catalan and coworkers showed that the ground-state tautomer form of **7AI** to be much more basic ($pK_a = 12$ for its conjugate acid) than the normal form ($pK_a = 5.5$ for its conjugate acid).²⁸ Assuming the tautomer of **7AI** and its N(7) methylated derivative, **7M7AI**, have similar excited-state photoacidity, the pK_a^* values are 10.3 for the **7AI** excited-state tautomer and 4.6 for the excited-state normal form (**Table 2**). It can be seen that the computational results for **7AI** tautomer in the ground-state and the experimental results for **7M7AI** have the same trend.

Table 3. The calculation of electron density distribution of N(1) and N(7) atoms in water for **7AI** and its analogues (See **Scheme 1** for their structures).

Compound	HOMO (ground state)	N(1)	N(7)
	LUMO (excited state)		
7AI	HOMO	9.15%	4.75%
	LUMO	1.05%	22.95%
3MAI	HOMO	12.54%	4.78%
	LUMO	0.78%	23.28%
3CAI	HOMO	8.91%	5.22%
	LUMO	3.17%	19.68%
2,7-diazaindole	HOMO	28.25%	12.60%
	LUMO	2.82%	19.00%
2CF₃AI	HOMO	10.46%	6.38%
	LUMO	2.74%	18.09%



Unification of the overall mechanism of ESPT


Generalization of the above acidity-basicity correlated proton-transfer tautomer emission requires support of other **7AI** derivatives. In 2001, we synthesized a **7AI** derivative, 3-cyano-7-azaindole (**3CAI**)²⁶, which revealed prominent proton-transfer emission at 480 nm (**Figure 9**), demonstrating that water catalyzed ESPT indeed takes place in pure H₂O (pH 7) for **3CAI**. We then synthesized the N(7)-CH₃ tautomer analogue of **3CAI**, namely 3-cyano-7-methyl-7*H*-pyrrolo[2,3-*b*]pyridine (**7M3CAI**, **Scheme 1**)²⁶ and measured the pK_a^* of **7M3CAI** (N(1)-H⁺) to be as low as 0.2 (**Table 2**), indicating that **7M3CAI** exists without protonation at pH 7. Likewise, assuming similar acid-base properties as **7M3CAI**, the proton-transfer tautomer of **3CAI**, i.e. the N(7)-H tautomer, is expected to exist in the excited state without protonation in neutral water, consistent with the observation of prominent green emission.²⁶

Chemically, the main difference between **7AI** and **3CAI** lies in the much higher acidity due to its strong electron-withdrawing -CN group at C(3) position, increasing the N(1)-H acidity. The water catalyzed pyrrolic N(1)-H → pyridyl N(7)-H proton transfer essentially results in the deprotonation of N(1)-H, forming a tautomer in which the imine N(1) nitrogen is a conjugate base of the N(1)-H⁺ acid. Accordingly, due to its

strong N(1)-H⁺ acidity, the basicity of N(1) nitrogen in the **3CAI** tautomer is expected to be much weaker (cf. **7AI** tautomer); therefore, protonation of **3CAI** tautomer is thermally unfavorable.



To further test the above viewpoint regarding thermodynamics governed deactivation of proton-transfer tautomer, we then provide several other **7AI** derivatives and their N(7)-CH₃ tautomer analogues, which are anchored by either electron-donating or withdrawing groups at the pyrrole site, and then carefully performed the spectroscopy and acidity (fluorescence titration) measurement. As a result, adding a methyl group at C(3) of **7AI**, forming **3MAI**, exhibits solely a normal emission band maximized at 420 nm (**Figure 9**) in neutral water. The pK_a^* of its tautomer analogue **7M3MAI** (**Scheme 1** and **Table 2**) in protonated form **7M3MAI** (N(1)-H⁺) is measured to be 9.4. Apply similar pK_a^* to **3MAI** proton transfer tautomer cation (N(1)-H⁺), the protonation of tautomer is expected, explaining the absence of tautomer emission in neutral water. Moreover, replacing C(2) by an electron-withdrawing N(2) nitrogen, we have reported a well resolved proton transfer emission in 500 nm for **(2,7-aza)Trp** in neutral water (vide supra).¹⁸ The prohibition of protonation on the **(2,7-aza)Trp** tautomer in the excited state well correlates with pK_a^* of 5.8 of its tautomer analogue **7M(2,7-aza)Trp**



(**Scheme 1** and **Table 2**) in the protonated form, **7M(2,7-aza)Trp** ($\text{N}(1)\text{-H}^+$). To provide additional example, we then add a substituent CF_3 at C(2) of **7AI** to form **2CF₃AI** (see **Scheme 1**), which also gives a well resolved tautomer emission at 500 nm (**Figure 9**).

The existence of tautomer and hence the prominent green emission implies the low $\text{p}K_{\text{a}}^*$ ($\ll 7$) of its conjugate acid. This is firmly supported by the $\text{p}K_{\text{a}}^*$ of as low as -0.3 for the protonated form of its methyl tautomer analogue **7M2CF₃AI** ($\text{N}(1)\text{-H}^+$).

Therefore, the results conclude that for those derivatives with electron-donating substituent (including $-\text{H}$) at C(3), following water catalyzed ESPT to form an excited $\text{N}(7)\text{-H}$ proton-transfer tautomer, rapid protonation takes place to generate an excited cationic species at pH 7. Conversely, protonation of the tautomer is thermally unfavorable in the excited state for those derivatives with electron-withdrawing substituent at C(2) or C(3), or C(2) replaced with an electron-withdrawing nitrogen atom, giving a prominent green emission.

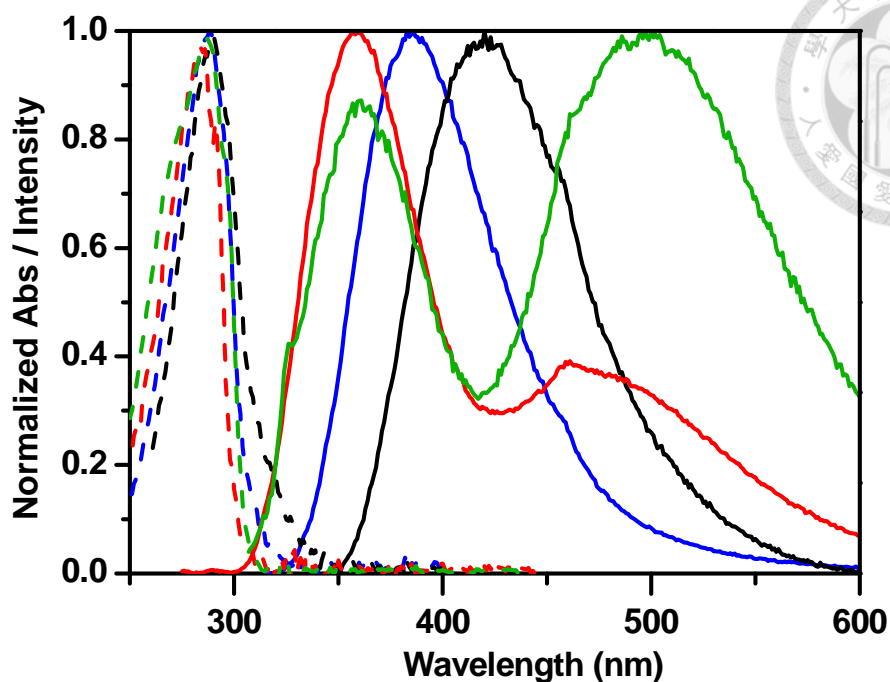


Figure 9. Steady-state absorption (dashed lines) and emission spectra (solid lines) for **7AI** (blue), **3MAI** (black), **2CF₃AI** (green), **3CAI** (red) in neutral water at room temperature.

We then make attempts to combine the water catalyzed ESPT mechanisms for **7AI**, which are respectively proposed by Petrich⁶ and Maroncelli¹⁰ with certain dissimilarity, and make one step further to bring up a generalized mechanism applicable to all titled **7AI** derivatives in neutral water. First of all, we adopt Chapman and Maroncelli's ESPT mechanism¹⁰ in that the entire **7AI**, rather than a small portion of **7AI** proposed by Petrich and co-workers⁶, undergo water catalyzed ESPT. Accordingly, polysolvated **7AI** are the predominant species in the ground state, which upon electronic excitation have

to form the 1:1 **7AI**/water cyclic H-bond complex (**Figure 10**) prior to proton transfer.

To rationalize the deuterium isotope effect, Chapman and Maroncelli¹⁰ further proposed

the existence of pre-equilibrium between polysolvated **7AI** and **7AI**/water cyclic

H-bond complex, in which forming the **7AI**/water cyclic H-bond complex is an

endergonic process. This is reasonable because molecular dynamics approach has

concluded that the equilibrium toward the **7AI**-water cyclic form is negligible and has

to be formed in the excited state via thermal activation prior to executing proton

transfer²⁹⁻³¹. Using a steady state approach, the rate of ESPT, k_{rxn} , to form a tautomer in

the excited can be expressed by

$$k_{\text{rxn}} = k_{\text{pt}} e^{-\Delta G^\ddagger/RT} \quad (\text{Eq. 2})$$

where G^\ddagger is the difference in free energy between polysolvated **7AI** and **7AI**/water

cyclic H-bond complex. Note that G^\ddagger is not an activation free energy but a true

equilibrium free energy. k_{pt} may be treated as a proton tunneling rate constant and hence

is expected to be deuterium isotope dependent. As a result, being different from

conventional wisdom, the slope of k_{rxn} as a function of $1/T$ is deuterium isotope


independent, while the extrapolation to $1/T \sim 0$ is deuterium isotope dependent. This

pre-equilibrium reaction dynamics has been supported by the deuterium isotope studies of ESPT in the case of **3CAI**.²⁶



Upon forming the proton transfer tautomer species in the excited state (the N(7)-H isomer denoted as T*, see **Figure 10**), we then adopt Petrich's model in that the thermodynamic property of **7AI** proton-transfer tautomer T* (see **Figure 10**) plays a key role to decide its relaxation pathways in water. We also prove in this study that this is generally applicable to all **7AI** derivatives. The core of the model lies in the acidity scale of the N(7)-H cationic form in the excited state. In neutral water (pH 7), if pK_a^* of the tautomer cation form (denoted as TC*, see **Figure 10**) is < 7 , T* should not be protonated. One thus expects to observe tautomer T* emission. Conversely, for pK_a^* of TC* > 7 , the tautomer T* emission is not observable due to the protonation of T* at the -N(1) site (i.e., forming a TC*, see **Figure 10**).

Using **7AI** as a prototype, we were not able to resolve TC* emission in both steady-state and kinetic manners (vide supra). As for another case, 3-methyl-7-azaindole (**3MAI**) also exhibits solely the normal emission (**Figure 9**), and similarly neither tautomer (T*) nor its cationic emission could be resolved. In the early section we have tentatively proposed the excited tautomer cationic (TC*) species to be an intermediate,



which deactivates to certain ground-state species in a rate much faster than its formation. Kinetically, this implies that the population of the excited tautomer cation (T^*) achieves a steady state and its concentration, and hence emission, is too low to be resolved. From chemistry point of view, the tautomer cation (TC^*) has the same canonical structure as the cation of the normal species ($N(7)-H^+$, see **Figure 11**). Thus, one plausible deactivation pathway is the internal conversion from TC^* to the ground state of the normal cation ($N(7)-H^+$). Due to the same canonical structure and hence the great vibronic overlaps, their state mixing must be very strong. In terms of quantum mechanics, if resonance should occur, the electron motion is no longer defined just zero-order function alone (ψ_1 or ψ_2), but a mixed state ($\psi_1 + \psi_2$). Such deactivation only requires the redistribution of the electron density and should be much faster than the rate of cation formation, i.e., k_{H^+} (**Figure 11**). As a result, the tautomer cationic (TC^*) emission is too weak to be resolved. Upon forming the normal cation ($N(7)-H^+$) in the ground state, due to the low pK_a value of 4.5 and 4.8 for protonated **7AI** and **3MAI**, respectively (see **Table 2**), further deprotonation takes place in neutral water to get back to the normal ground state, achieving a proton transfer cycle.

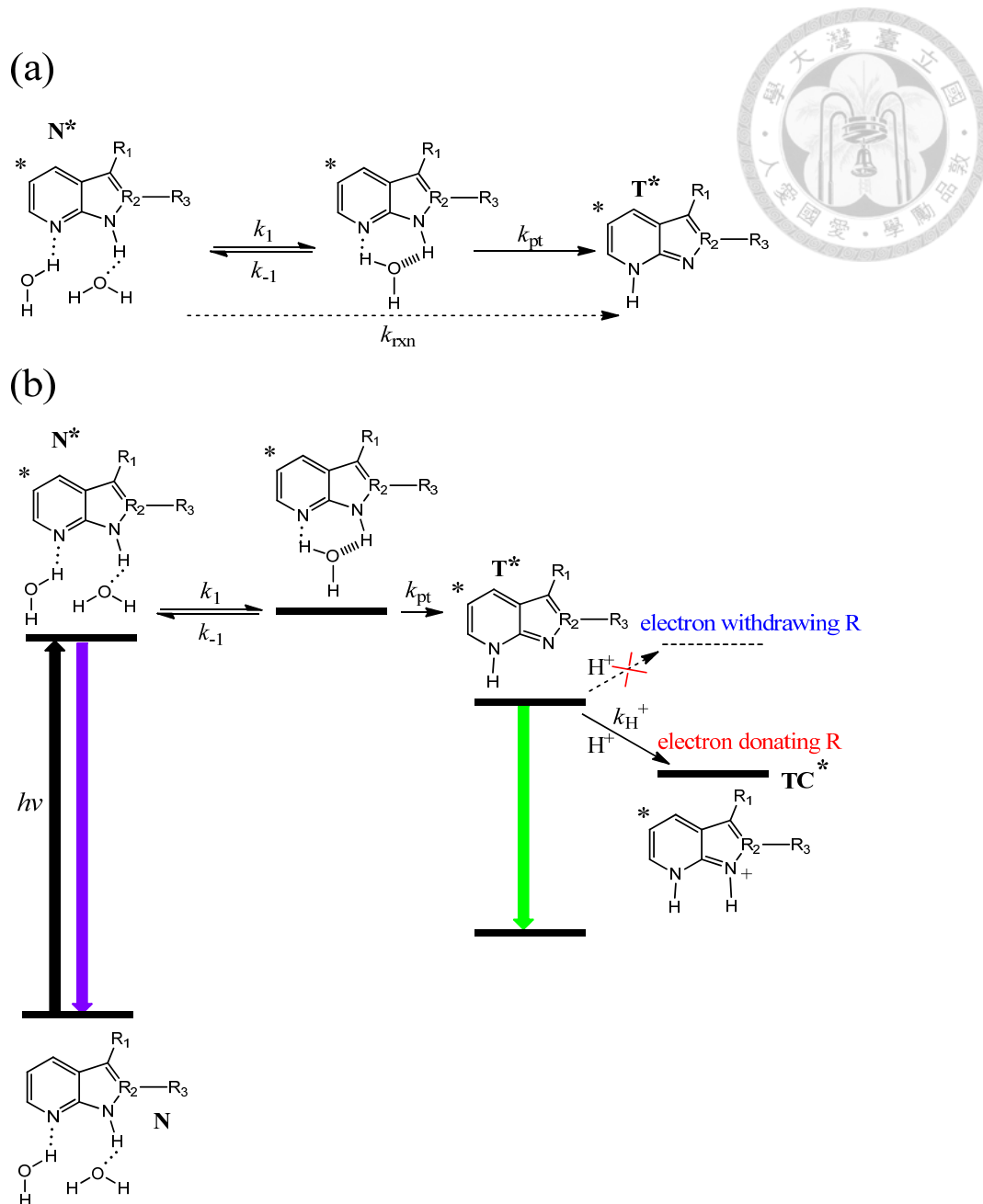


Figure 10. (a) The proposed water catalyzed ESPT for **7AI** derivatives. (b) The mechanism of water catalyzed ESPT and the following deactivation pathways for **7AI** derivatives in the neutral water. The asterisk * indicates the electronic excited state.

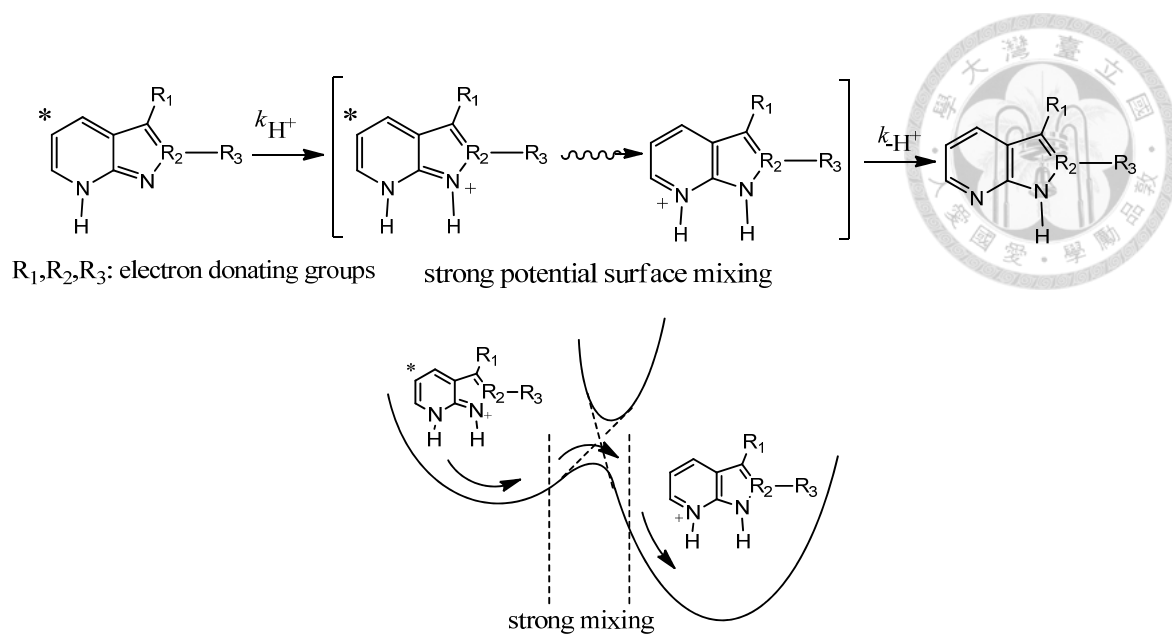


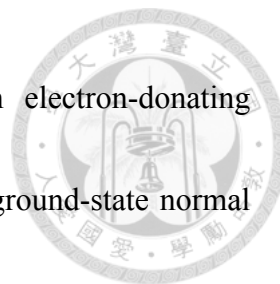
Figure 11. The proposed deactivation pathway of the proton-transfer tautomer cation in the excited state. The asterisk $*$ denotes the electronic excited state.

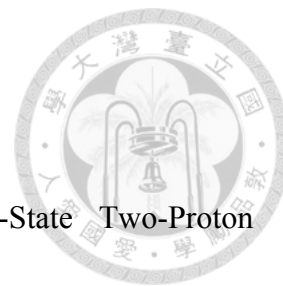


4. Conclusion

In sum, we have carried out the fluorometric pH titration, in combination with the corresponding relaxation dynamics, to resolve the proton-transfer tautomer 530 nm emission of **7AI** within a narrow basic range of pH 13.0-14.5. This explains why the tautomer emission of **7AI** has not been observed in neutral water during the past decades, whereas the tautomer emission is very prominent in e.g. alcohol solvents.^{5,7} Realizing that the acid-base property of the tautomer is key for its excited-state deactivation process, we then systematically study a series of **7AI** analogues and their methylated derivatives on pK_a , pK_a^* , together with the associated fluorescence spectroscopy and dynamics. The results conclude that all **7AI** derivatives undergo water catalyzed ESPT in neutral water. For those derivatives with electron-donating substituent (including -H) at C(3), following water catalyzed ESPT to form an excited proton-transfer tautomer, T^* , rapid protonation takes place to generate an excited cationic species, TC^* , due mainly to the $pK_a^* \gg 7$ for the cation form of T^* . Conversely, protonation in T^* is prohibited (pK_a^* of $TC^* < 7$) for those derivatives with electron-withdrawing substituent at C(2) or C(3), or C(2) replaced with an electron-withdrawing nitrogen atom (N(2) in e.g., 2,7-diazatryptophan), giving a

prominent green T* emission. For those **7AI** derivatives with electron-donating substituent, the tautomer cation undergoes fast deactivation to the ground-state normal cationic form, followed by deprotonation to the original normal species to wrap up a proton transfer cycle. The information gathered is thus valuable for future strategic design of the tryptophan analogues as an ideal probe for sensing water in proteins.¹⁸





5. References

- (1) Taylor, C. A.; Elbayoumi, M. A.; Kasha, M. Excited-State Two-Proton Tautomerism in Hydrogen-Bonded N-Heterocyclic Base Pairs. *Proc. Natl. Acad. Sci. U.S.A.* **1969**, *63*, 253.
- (2) Watson, J. D.; Crick, F. H. C. Molecular Structure of Nucleic Acids - a Structure for Deoxyribose Nucleic Acid. *Nature* **1953**, *171*, 737.
- (3) Doudney, C. O.; Rinaldi, C. N. Evidence That Ultraviolet Light-Induced DNA-Replication Death of recA Bacteria Is Prevented by Protein-Synthesis in Repair-Proficient Bacteria. *Mutat. Res.* **1989**, *217*, 33.
- (4) Ingham, K. C.; Elbayoumi, M. A. Photoinduced Double Proton-Transfer in a Model Hydrogen-Bonded Base Pair - Effects of Temperature and Deuterium Substitution. *J. Am. Chem. Soc.* **1974**, *96*, 1674.
- (5) Moog, R. S.; Maroncelli, M. 7-Azaindole in Alcohols - Solvation Dynamics and Proton-Transfer. *J. Phys. Chem.* **1991**, *95*, 10359.
- (6) Chen, Y.; Rich, R. L.; Gai, F.; Petrich, J. W. Fluorescent Species of 7-Azaindole and 7-Azatryptophan in Water. *J. Phys. Chem.* **1993**, *97*, 1770.



(7) McMorrow, D.; Aartsma, T. J. Solvent-Mediated Proton-Transfer the Roles of Solvent Structure and Dynamics on the Excited-State Tautomerization of 7-Azaindole/Alcohol Complexes. *Chem. Phys. Lett.* **1986**, *125*, 581.

(8) Takeuchi, S.; Tahara, T. Observation of Dimer Excited-State Dynamics in the Double Proton Transfer Reaction of 7-Azaindole by Femtosecond Fluorescence Up-Conversion. *Chem. Phys. Lett.* **1997**, *277*, 340.

(9) Takeuchi, S.; Tahara, T. The Answer to Concerted versus Step-Wise Controversy for the Double Proton Transfer Mechanism of 7-Azaindole Dimer in Solution. *Proc. Natl. Acad. Sci. U.S.A.* **2007**, *104*, 5285.

(10) Chapman, C. F.; Maroncelli, M. Excited-State Tautomerization of 7-Azaindole in Water. *J. Phys. Chem.* **1992**, *96*, 8430.

(11) Negreie, M.; Bellefeuille, S. M.; Whitham, S.; Petrich, J. W.; Thornburg, R. W. Novel Noninvasive in Situ Probe of Protein-Structure and Dynamics. *J. Am. Chem. Soc.* **1990**, *112*, 7419.

(12) Negreie, M.; Gai, F.; Bellefeuille, S. M.; Petrich, J. W. Photophysics of a Novel Optical Probe : 7-Azaindole. *J. Phys. Chem.* **1991**, *95*, 8663.



(13) Gai, F.; Chen, Y.; Petrich, J. W. Nonradiative Pathways of 7-Azaindole in Water. *J. Am. Chem. Soc.* **1992**, *114*, 8343.

(14) Abel, R.; Salam, N. K.; Shelley, J.; Farid, R.; Friesner, R. A.; Sherman, W. Contribution of Explicit Solvent Effects to the Binding Affinity of Small-Molecule Inhibitors in Blood Coagulation Factor Serine Proteases. *ChemMedChem* **2011**, *6*, 1049.

(15) Robinson, D. D.; Sherman, W.; Farid, R. Understanding Kinase Selectivity Through Energetic Analysis of Binding Site Waters. *ChemMedChem* **2010**, *5*, 618.

(16) Beuming, T.; Che, Y.; Abel, R.; Kim, B.; Shanmugasundaram, V.; Sherman, W. Thermodynamic Analysis of Water molecules at the Surface of Proteins and Applications to Binding Site Prediction and Characterization. *Proteins* **2012**, *80*, 871.

(17) Wang, L.; Berne, B. J.; Friesner, R. A. Ligand Binding to Protein-Binding Pockets with Wet and Dry Regions. *Proc. Natl. Acad. Sci. U. S. A.* **2011**, *108*, 1326.

(18) Shen, J. Y.; Chao, W. C.; Liu, C.; Pan, H. A.; Yang, H. C.; Chen, C. L.; Lan, Y. K.; Lin, L. J.; Wang, J. S.; Lu, J. F.; Chou, S. C. W.; Tang, K. C.; Chou, P. T. Probing Water Micro-Solvation in Proteins by Water Catalysed Proton-Transfer Tautomerism. *Nat. Commun.* **2013**, *4*, 2611.

(19) Chou, P. T.; Chen, Y. C.; Yu, W. S.; Chou, Y. H.; Wei, C. Y.; Cheng, Y. M.
Excited-State Intramolecular Proton Transfer in 10-Hydroxybenzo[h]quinoline *J. Phys.*

Chem. A **2001**, *105*, 1731.

(20) Chou, P. T.; Pu, S. C.; Cheng, Y. M.; Yu, W. S.; Yu, Y. C.; Hung, F. T.; Hu, W. P.

Femtosecond Dynamics on Excited-State Proton Charge-Transfer Reaction in
4'-N,N-Diethylamino-3-hydroxyflavone. The Role of Dipolar Vectors in Constructing a

Rational Mechanism. *J. Phys. Chem. A* **2005**, *109*, 3777.

(21) Frisch, M. J.; Trucks, G. W.; Schlegel, H. B.; Scuseria, G. E.; Robb, M. A.;

Cheeseman, J. R.; Scalmani, G.; Barone, V.; Mennucci, B.; Petersson, G. A.; et al.

Gaussian 09, revision A.02; Gaussian, Inc.: Wallingford, CT, **2009**.

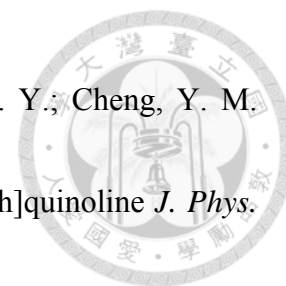
(22) Avouris, P.; Yang, L. L.; Elbayoumi, M. A. Excited-State Interactions of

7-Azaindole with Alcohol and Water. *Photochem. Photobiol.* **1976**, *24*, 211.

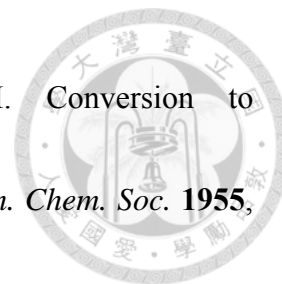
(23) Chou, P. T.; Martinez, M. L.; Cooper, W. C.; McMorro, D.; Collins, S. T.; Kasha,

M. Monohydrate Catalysis of Excited-State Double-Proton Transfer in 7-Azaindole. *J.*

Phys. Chem. **1992**, *96*, 5203.



(24) Robison, M. M.; Robison, B. L. 7-Azaindole. II. Conversion to 7-Methyl-7H-pyrrolo[2,3-b]pyridine and Related Compounds. *J. Am. Chem. Soc.* **1955**, *77*, 6554.



(25) Yu, W. S.; Cheng, C. C.; Chang, C. P.; Wu, G. R.; Hsu, C. H.; Chou, P. T. Excited-State Double-Proton Transfer on 3-Methyl-7-azaindole in a Single Crystal: Deuterium Isotope/Tunneling Effect. *J. Phys. Chem. A* **2002**, *106*, 8006.

(26) Chou, P. T.; Yu, W. S.; Wei, C. Y.; Cheng, Y. M.; Yang, C. Y. Water-Catalyzed Excited-State Double Proton Transfer in 3-Cyano-7-azaindole: The Resolution of the Proton-Transfer Mechanism for 7-Azaindoles in Pure Water. *J. Am. Chem. Soc.* **2001**, *123*, 3599.

(27) Carnerero, J. M.; Gonzalez-Benjumea, A.; Carmona, C.; Balon, M. Spectroscopic Study of the Ground and Excited State Prototropic Equilibria of 4-azaindole. *Spectrochim. Acta. A* **2012**, *97*, 1072.

(28) Catalan, J.; Mo, O.; Perez, P.; Yanez, M. Influence of the Tautomeric Forms of Azaindoles on Their Basicity in Solution. *Theochem. J. Mol. Struc.* **1984**, *16*, 263.



(29) Mente, S.; Maroncelli, M. Solvation and the Excited-State Tautomerization of 7-Azaindole and 1-Azacarbazole: Computer Simulations in Water and Alcohol Solvents.

J. Phys. Chem. A **1998**, *102*, 3860.

(30) Kyrychenko, A.; Waluk, J. Excited-State Proton Transfer through Water Bridges and Structure of Hydrogen-Bonded Complexes in 1H-Pyrrolo[3,2-h] quinoline:

Adiabatic Time-Dependent Density Functional Theory Study. *J. Phys. Chem. A* **2006**, *110*, 11958.

(31) Kyrychenko, A.; Stepanenko, Y.; Waluk, J. Molecular Dynamics and DFT Studies of Intermolecular Hydrogen Bonds between Bifunctional Heteroazaaromatic Molecules and Hydroxylic Solvents. *J. Phys. Chem. A* **2000**, *104*, 9542.

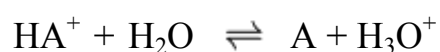


6. Supporting Information

Determination of ground state dissociation constants (pK_a) by UV spectroscopy

The dissociation constant of the compound, pK_a , is a measure of acid strength of the compound, and the pH above the pK_a value result that the compound is mostly anion or neutral, and below the pK_a value result that the compound is mostly neutral or cation. Therefore, this constant has an important role in estimating behavior of the compound in various pH-conditions.

We show the relationship of pH and pK_a in the below:




$$K_a = \frac{[H_3O^+][A]}{[HA^+]}$$

$$pH = pK_a + \log \frac{[A]}{[HA^+]}$$

$$[A] = [HA^+] \rightarrow pH = pK_a$$

Determination of the pK_a value by use spectrophotometric titration, where a UV spectrum of the compound is taken for each point of the titration and the change in UV absorbance of the specific wavelength is plotted against the pH. The specific wavelength is not absorbance in most high or most low pH. In other words, the cation or neutral form is not absorbance in the specific wavelength. Therefore, the absorbance of



specific wavelength is linear relationship with the concentration of another component, such as cation or neutral form. The half of absorbance maximum of the specific wavelength is deliver that the concentration of the cation and neutral form is equal and the pH value is pK_a .

Determination of excited state dissociation constants (pK_a^*) by fluorescence spectroscopy

Determination of the pK_a^* value by use fluorescence titration, where a fluorescence spectrum of the compound is taken for each point of the titration and the change in fluorescence intensity of the specific wavelength is plotted against the pH. If the proton transfer equilibrium is not rapid on the time scale of the excited-state lifetimes, then titration curves based on fluorescence measurements will not accurately measure the excited-state pK_a^* . We just use the pK_a^* value to determinate the possibility of protonated of tautomer, therefore, the deviation is not affect our result.

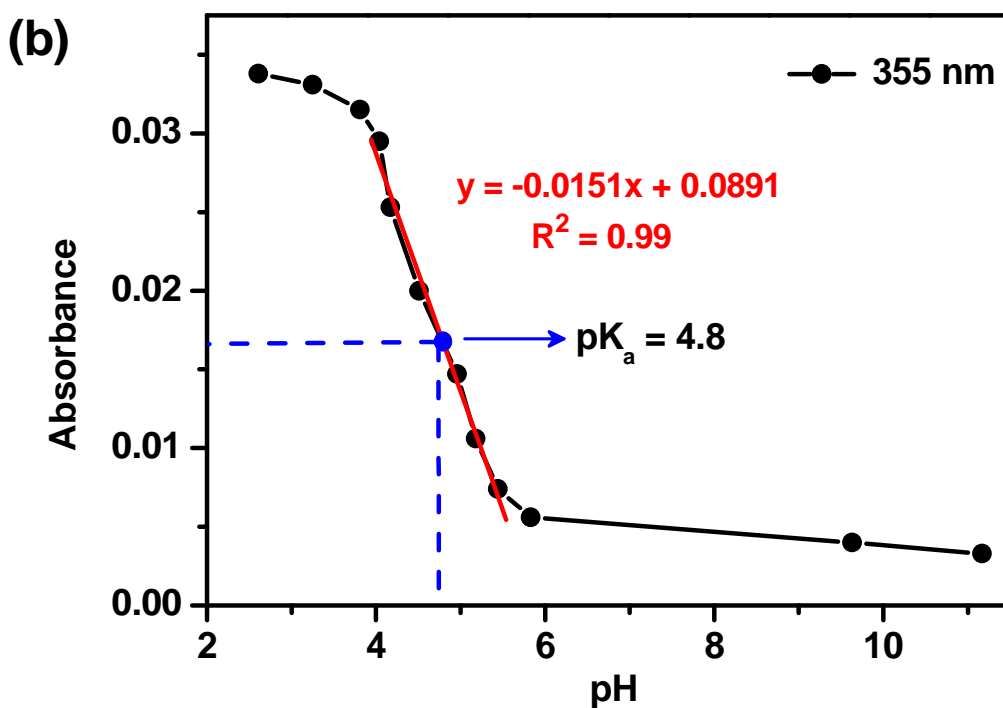
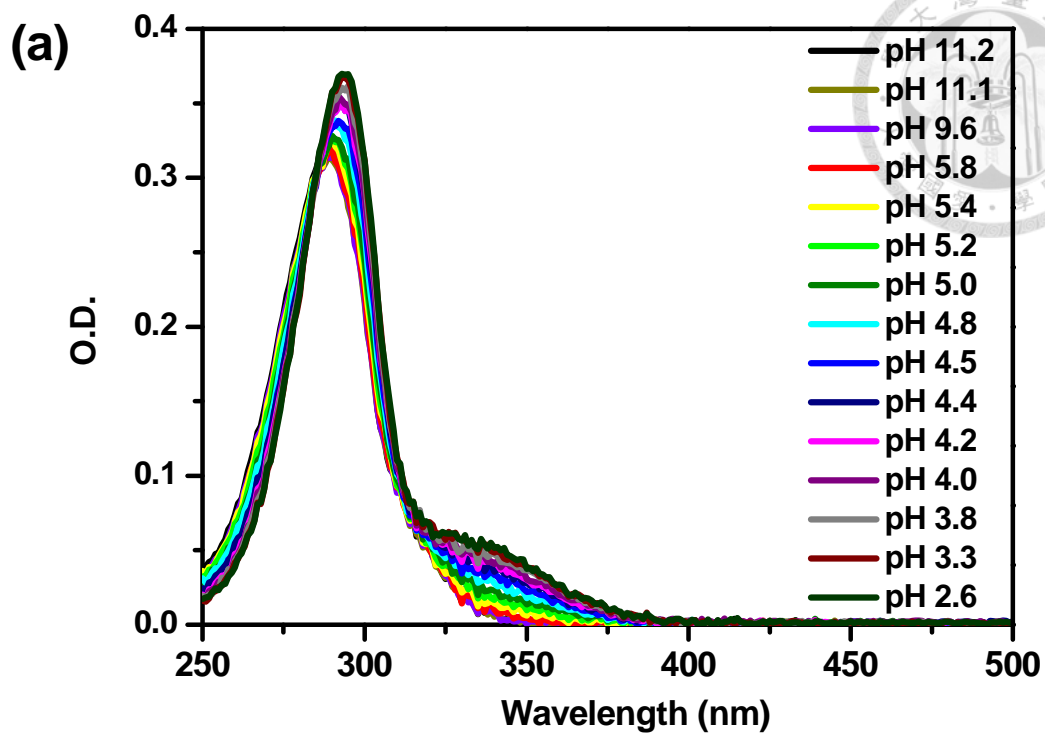


Figure S1. Spectral data analysis and pK_a determination. (a) Steady-state absorption spectrum of 3MAI in different pH value. (b) Plot of the absorbance of 355 nm vs. pH to determine the pK_a .

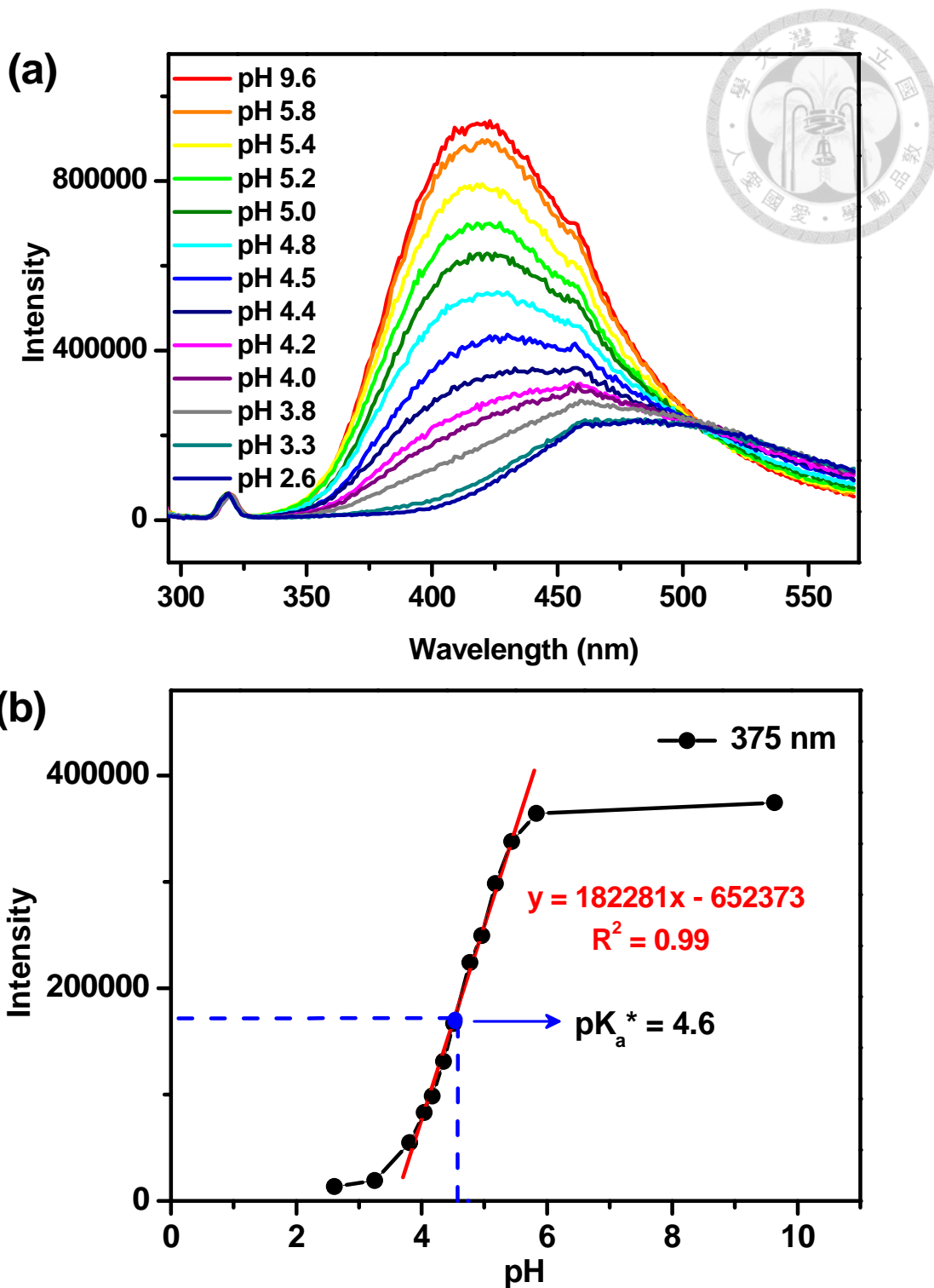


Figure S2. Spectral data analysis and pK_a^* determination. (a) Steady-state emission spectrum of 3MAI in different pH value with 285 nm excitation. (b) Plot of the emission intensity of 375 nm vs. pH to determine the pK_a^* .

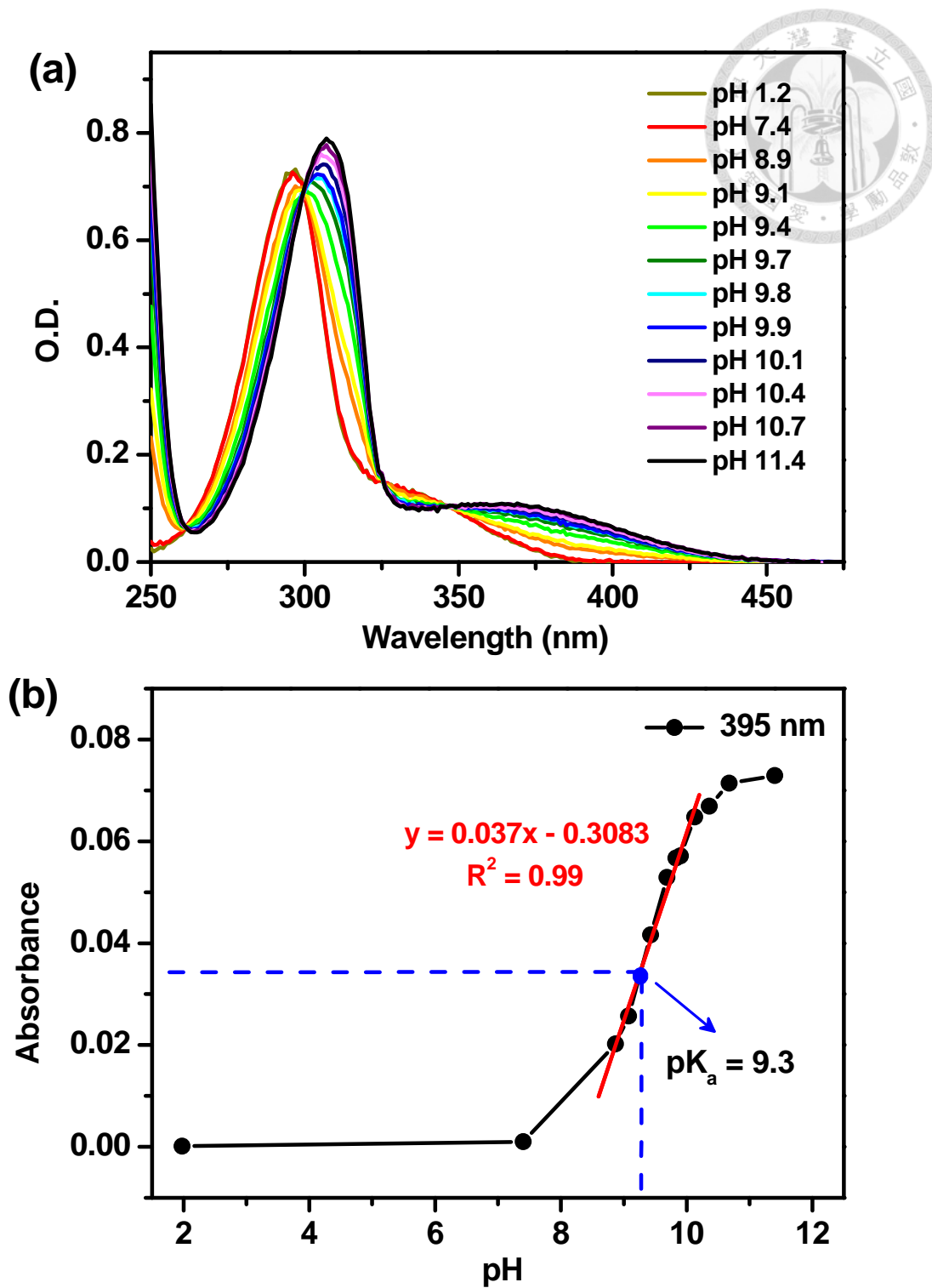


Figure S3. Spectral data analysis and pK_a determination. (a) Steady-state absorption spectrum of 7M3MAI in different pH value. (b) Plot of the absorbance of 395 nm vs. pH to determine the pK_a .

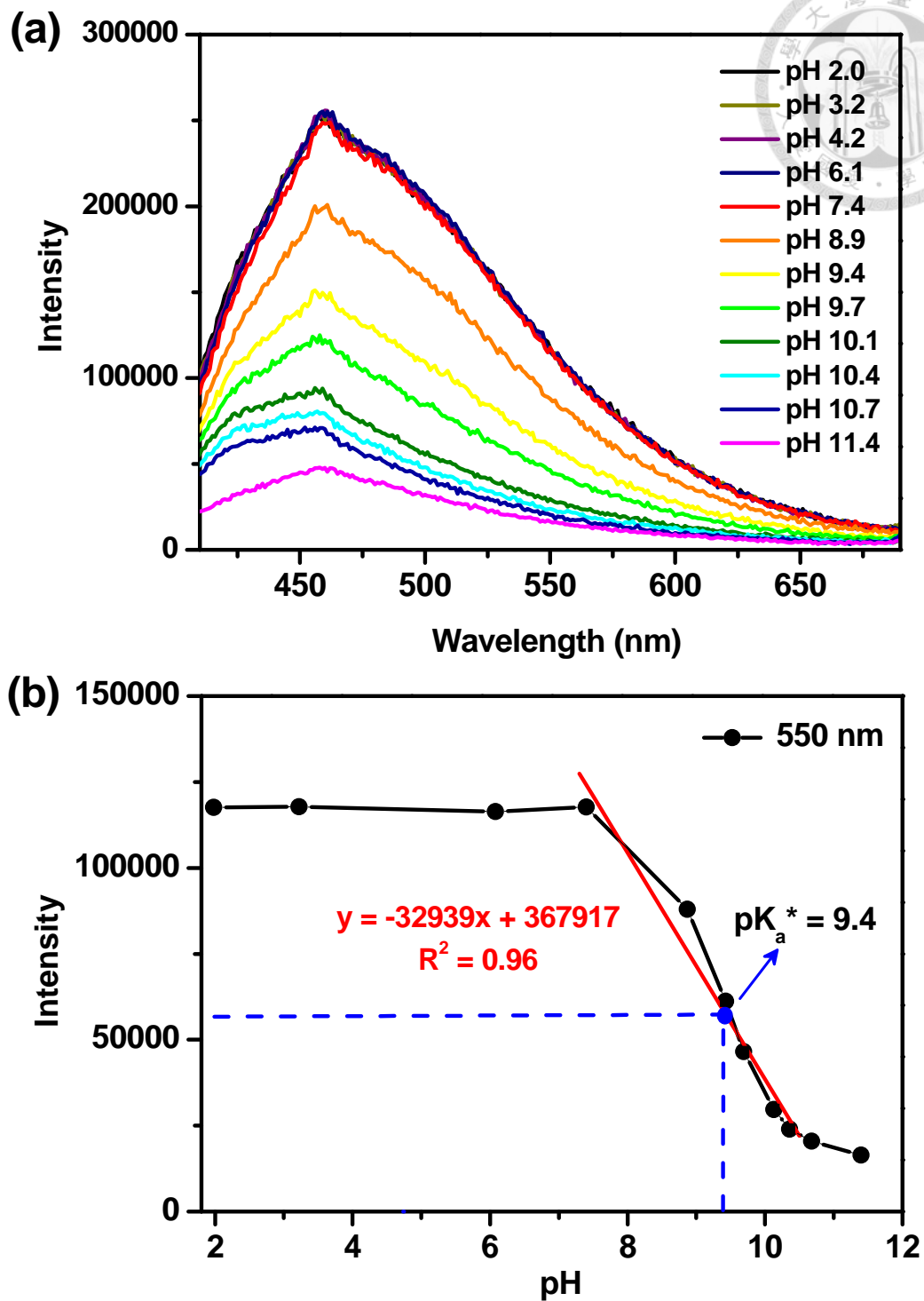


Figure S4. Spectral data analysis and pK_a^* determination. (a) Steady-state emission spectrum of 7M3MAI in different pH value with 350 nm excitation. (b) Plot of the emission intensity of 550 nm vs. pH to determine the pK_a^* .

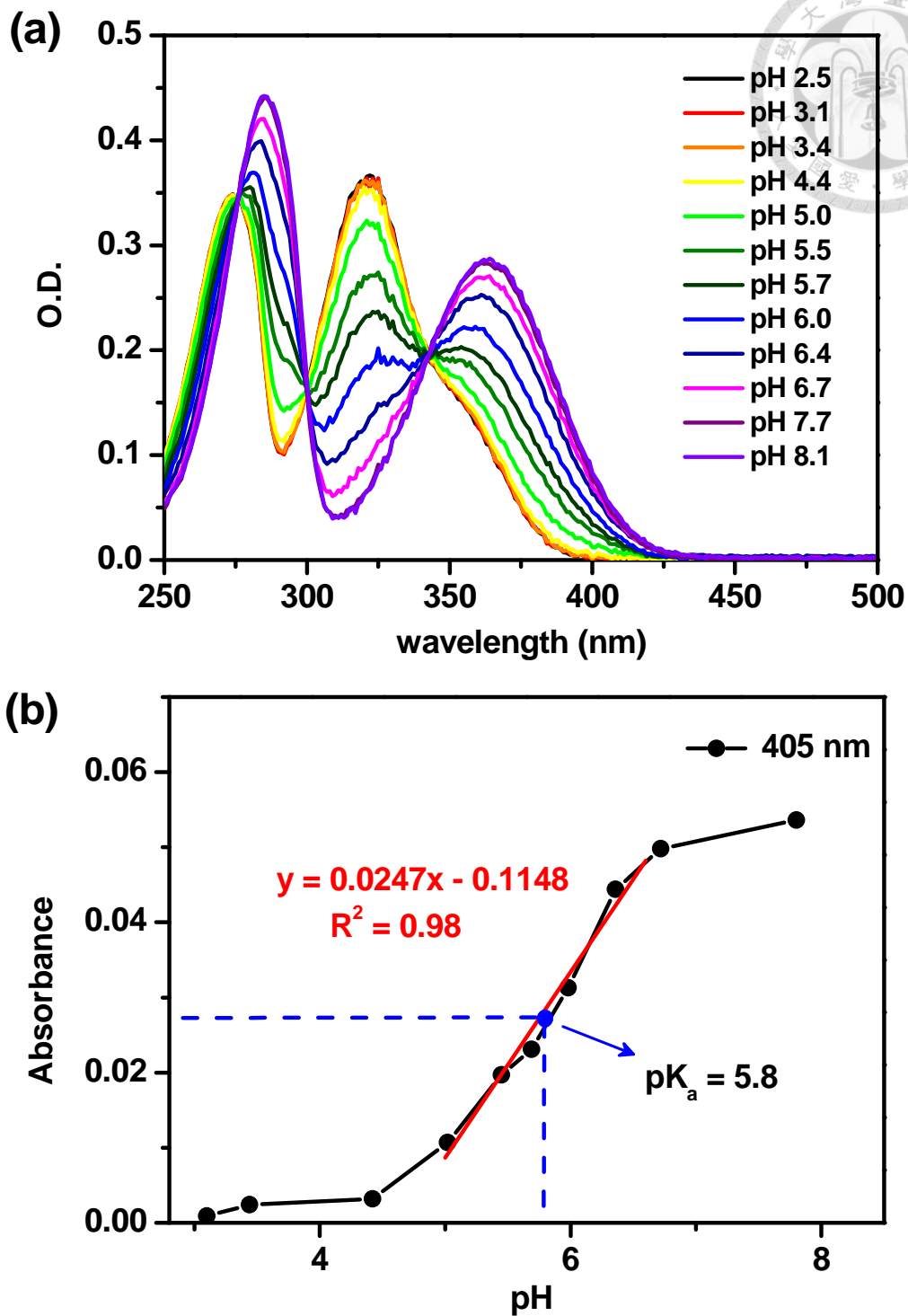


Figure S5. Spectral data analysis and pK_a determination. (a) Steady-state absorption spectrum of 7M(2,7-aza)Trp in different pH value. (b) Plot of the absorbance of 405 nm vs. pH to determine the pK_a .

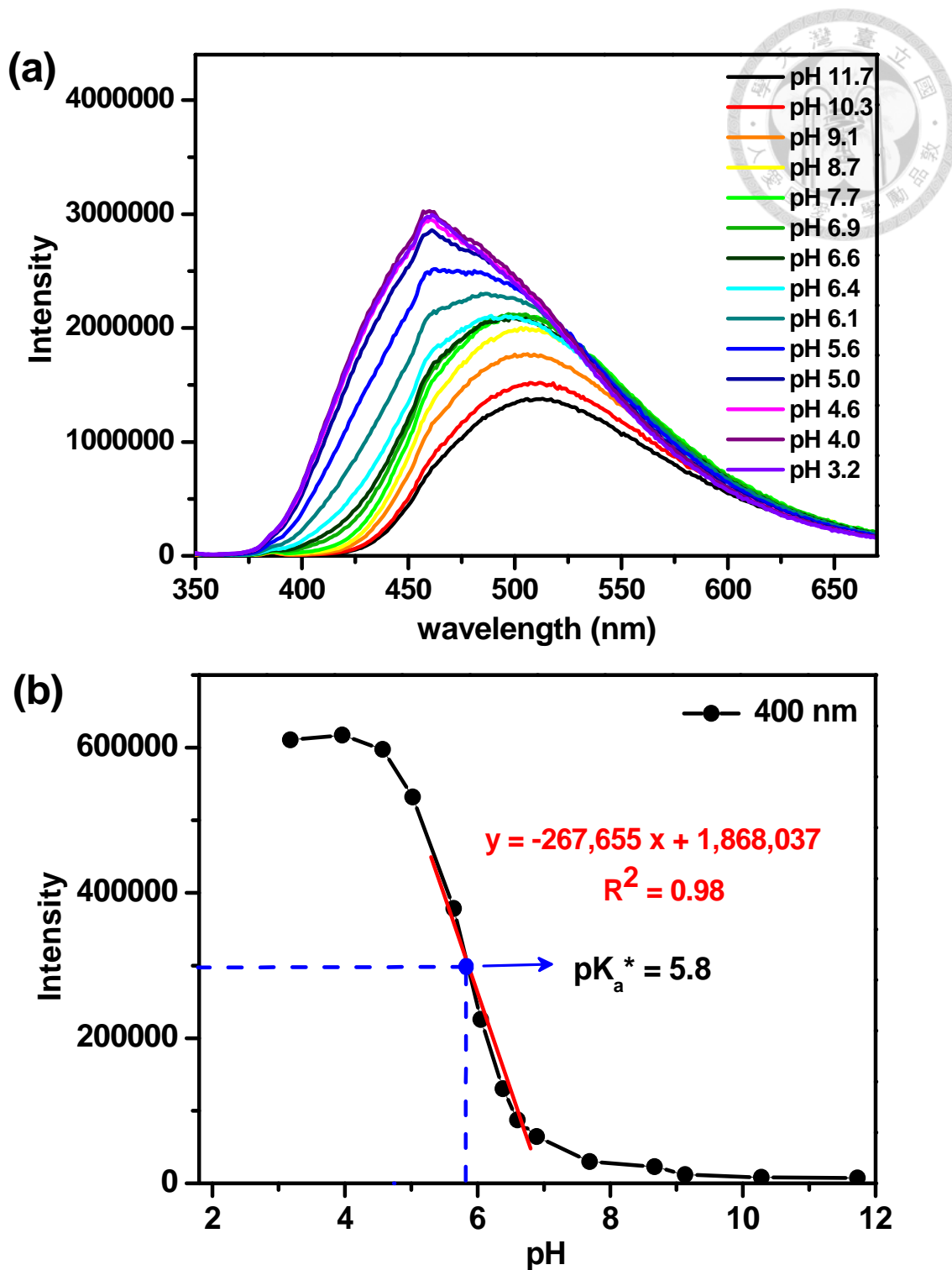


Figure S6. Spectral data analysis and pK_a^* determination. (a) Steady-state emission spectrum of 7M(2,7-aza)Trp in different pH value with 342 nm excitation. (b) Plot of the emission intensity of 400 nm vs. pH to determine the pK_a^* .

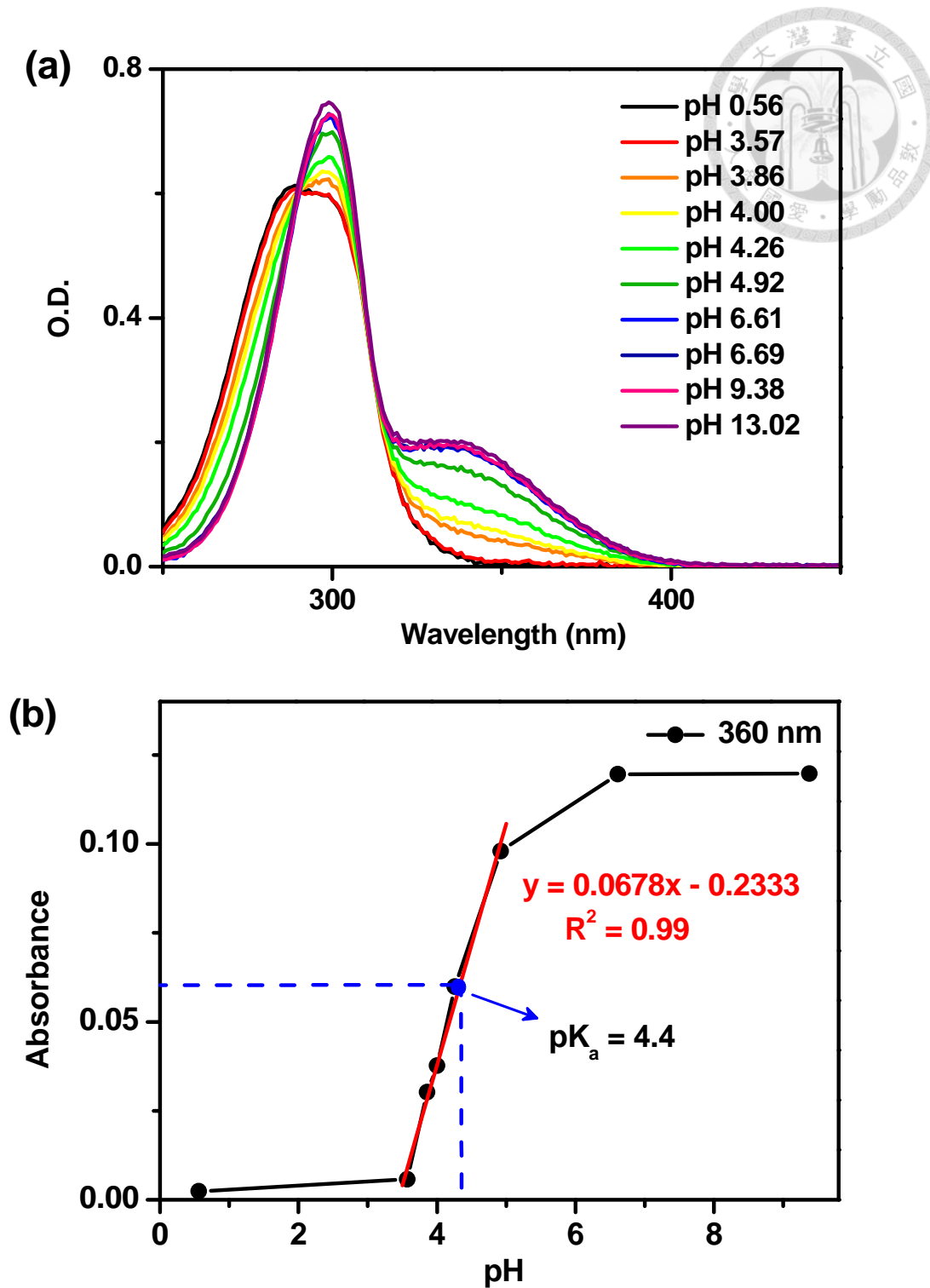


Figure S7. Spectral data analysis and pK_a determination. (a) Steady-state absorption spectrum of 7M2CF₃AI in different pH value. (b) Plot of the absorbance of 360 nm vs. pH to determine the pK_a.

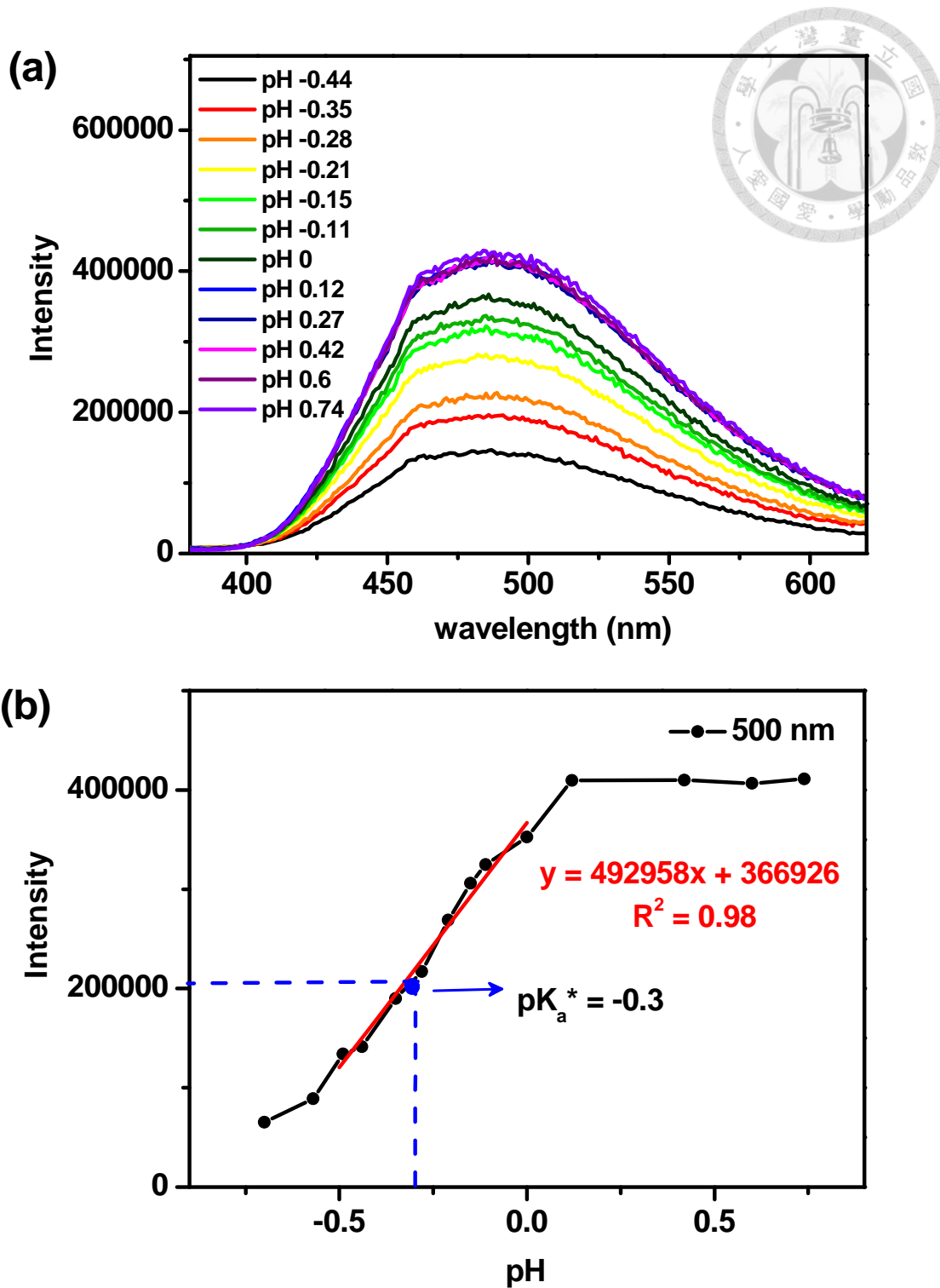


Figure S8. Spectral data analysis and pK_a^* determination. (a) Steady-state emission spectrum of 7M2CF₃AI in different pH value with 315 nm excitation. (b) Plot of the emission intensity of 500 nm vs. pH to determine the pK_a^* .